© 2015. Published by The Company of Biologists Ltd | The Journal of Experimental Biology (2015) 218, 1099-1110 doi:10.1242/jeb.114868

RESEARCH ARTICLE

Mechanical challenges to freshwater residency in sharks and rays

Adrian C. Gleiss[1,2,*], Jean Potvin[3], James J. Keleher[1], Jeff M. Whitty[1], David L. Morgan[1] and Jeremy A. Goldbogen[2]

ABSTRACT

Major transitions between marine and freshwater habitats are relatively infrequent, primarily as a result of major physiological and ecological challenges. Few species of cartilaginous fish have evolved to occupy freshwater habitats. Current thought suggests that the metabolic physiology of sharks has remained a barrier to the diversification of this taxon in freshwater ecosystems. Here, we demonstrate that the physical properties of water provide an additional constraint for this species-rich group to occupy freshwater systems. Using hydromechanical modeling, we show that occurrence in fresh water results in a two- to three-fold increase in negative buoyancy for sharks and rays. This carries the energetic cost of lift production and results in increased buoyancy-dependent mechanical power requirements for swimming and increased optimal swim speeds. The primary source of buoyancy, the lipid-rich liver, offers only limited compensation for increased negative buoyancy as a result of decreasing water density; maintaining the same submerged weight would involve increasing the liver volume by very large amounts: 3- to 4-fold in scenarios where liver density is also reduced to currently observed minimal levels and 8-fold without any changes in liver density. The first data on body density from two species of elasmobranch occurring in freshwater (the bull shark *Carcharhinus leucas*, Müller and Henle 1839, and the largetooth sawfish *Pristis pristis*, Linnaeus 1758) support this hypothesis, showing similar liver sizes as marine forms but lower liver densities, but the greatest negative buoyancies of any elasmobranch studied to date. Our data suggest that the mechanical challenges associated with buoyancy control may have hampered the invasion of freshwater habitats in elasmobranchs, highlighting an additional key factor that may govern the predisposition of marine organisms to successfully establish in freshwater habitats.

KEY WORDS: Buoyancy, Liver, Tissue density, Locomotion, Lift, Drag

INTRODUCTION

A wide range of physiological, ecological and evolutionary processes determine the capacity of animals to invade and adapt to novel environments. For major transitions, such as those between aquatic and terrestrial or marine and fresh water environments, successful invasions are relatively infrequent in most plant and animal taxa, except for tetrapods (Vermeij and Dudley, 2000). However, transitions from saltwater to freshwater habitats can facilitate radiation and speciation events, which in some systems manifest as rapid and repeated invasions worldwide (Lee and Bell, 1999). The Chondrichthyes have proven relatively unsuccessful at invading freshwater habitats despite their worldwide distribution in marine ecosystems. Of the >1000 species of the Elasmobranchii, only approximately 5% are thought to reside in fresh water (Ballantyne and Fraser, 2013; Martin, 2005). Moreover, most of these species only utilize freshwater habitats for part of their life cycle.

The mechanism behind this stark pattern in biogeography has received significant attention in the literature for the last half century (e.g. Ballantyne and Robinson, 2010; Ballantyne and Fraser, 2013; Pillans and Franklin, 2004; Thorson, 1962); current hypotheses suggest that metabolic organisation of elasmobranchs is responsible for their poor penetration into fresh water, resulting in metabolic costs associated with osmoregulation (Ballantyne and Robinson, 2010; Meloni et al., 2002). Whereas the difference in solute concentrations has a significant impact on the physiological biochemistry of elasmobranchs, the potential impact of the changing density of sea water and fresh water has not been adequately considered. Although the difference in density between sea water (SW ~1026 kg m^{-3} at 20°C) and fresh water (FW ~996 kg m^{-3} at 20°C) may seem trivial, it could nevertheless have significant ramifications for the buoyancy control of these animals. Animal tissue is generally denser than both sea water and fresh water, so that marine animals without any organ providing buoyancy would be heavily negatively buoyant (Alexander, 1990; Davenport, 1999; Pelster, 2009). Elasmobranchs utilize lipid-rich livers to increase the buoyant force relative to their mass (commonly referred to as static lift) (Baldridge, 1970; Bone and Roberts, 1969; Corner et al., 1969). Because of the minor difference in density of liver tissue (900–1000 kg m^{-3}) compared with that of marine waters (~1027 kg m^{-3}), large livers are required to provide necessary force to approach near-neutral buoyancy. Indeed, neutrally buoyant sharks, which are commonly found in the deep sea may have livers that comprise 30% of whole body volume (Corner et al., 1969) compared with only 1–7% swimbladder volume required to provide neutral buoyancy in ray-finned fishes (Alexander, 1966; Davenport, 1999; Weitkamp, 2008).

Despite the use of the liver as a means to increase buoyancy, the majority of elasmobranch species remain negatively buoyant (Baldridge, 1970; Bone and Roberts, 1969; Gleiss et al., 2011b). Counteracting this negative buoyancy represents one of the two major forces that govern the energetics of locomotion in aquatic environments (Alexander, 1990, 2003). In elasmobranchs, the heterocercal caudal fin and the pectoral fins and/or the body generate vertical forces that balance this negative buoyancy (Fish and Shannahan, 2000; Wilga and Lauder, 2002). This, in turn, results in drag due to lift by the body and pectoral fins (known as induced drag, Alexander, 1990, 2003) and causes the vortex jet of the heterocercal caudal fin to have a vertical component (Wilga and Lauder, 2002), making excessive negative buoyancy unfavorable. The use of a buoyancy organ, such as a large lipid-rich liver, reduces

[1]Freshwater Fish Group & Fish Health Unit, School of Veterinary & Life Sciences, Murdoch University, 90 South Street, Murdoch, Western Australia 6150, Australia. [2]Hopkins Marine Station, Stanford University, Pacific Grove, CA 93950, USA. [3]Department of Physics, Saint Louis University, St Louis, MO 63103, USA.

*Author for correspondence (adrian.gleiss@gmail.com)

Received 30 September 2014; Accepted 18 December 2014

The Journal of Experimental Biology (2015) 218, 1099-1110 doi:10.1242/jeb.114868

this cost, but increases parasite drag, because of greater surface area and reduced streamlining (Alexander, 1990). Negative buoyancy is favourable for those animals travelling fast whereas neutral buoyancy provided by large livers favours lower travel speeds, as a result of decreasing costs of lift production at higher speeds (Alexander, 1990). For instance, Greenland sharks (*Somniosus microcephalus*), which have substantial liver sizes and are close to neutral buoyancy, cruise at speeds of only 0.1 lengths s^{-1} (Watanabe et al., 2012). In contrast, sharks that are more negatively buoyant tend to travel at 0.2–0.7 lengths s^{-1} (Watanabe et al., 2012).

The close relationship between the locomotor performance and body density may represent a fundamental influence on the lifestyle of elasmobranchs (Bone and Roberts, 1969; Gleiss et al., 2011a) and a key aspect to understanding how the constraints of water density and buoyancy shape the lives of those species that occur in fresh water. However, this has received no attention in the literature thus far (Ballantyne and Robinson, 2010). In this paper, we aim to clarify the impact of changing water density on the buoyancy and energetics of elasmobranchs. We model the expected change in buoyancy by calculating the theoretical buoyancies of marine species of shark occurring in freshwater. We then simulate the required change in liver size and density to compensate for the decrease in environmental density and calculate the energetic costs associated with different hypothetical scenarios of compensation. In a second part of this work, we present the first measurements of buoyancy of two species of elasmobranchs naturally occurring in freshwater and compare them with marine forms.

RESULTS

Modelling the morphological implications of water density

Changes in water density drastically alter the submerged weight of an elasmobranch, in this case our modelled bull shark (Fig. 1), as calculated by Eqn 1 described in the Materials and methods. Submerged weight increases linearly with a decline of water density. A reduction of liver density to the low values observed in deep-sea sharks (920 kg m^{-3}) can offset this increase to brackish waters of density of 1022 kg m^{-3} (Fig. 1). An additional mode of compensating for the reduced environmental density is to change the size of the liver, with larger livers providing more upthrust. Assuming no adjustments in liver density, liver volume would have to increase 8-fold to maintain a similar submerged weight in freshwater as in marine waters (Fig. 1), resulting in a liver comprising ∼60% of whole body volume. In the hypothetical scenario where a shark has the ability to reduce its liver density, liver volume would only have to increase 3-fold, resulting in a liver comprising ∼35% of body volume, compared with 14% in marine waters, to achieve the same submerged weight. We have to note here that these calculations assume that all other tissues maintain the same volume. This assumption is discussed below.

Modelling the energetic consequences of salinity

Negative buoyancy compensation via lift production by the body, pectoral fins and heterocercal tail, and attendant metabolic costs, was carried out using a standard approach to aircraft performance modelling (see Eqns 2–6A and Dole, 1981; Pope, 1951). Components of this model were validated with the shear stress drag data of smooth dogfish (*Mustelus canis*) measured by Anderson et al. (2001) (see also the Materials and methods). Swimming performance is assessed here with the expended metabolic power (P_{total}) and cost of transport (COT) incurred from (parasite) drag production and from negative buoyancy compensation via lift (see Eqns 6A and 7). These metabolic costs

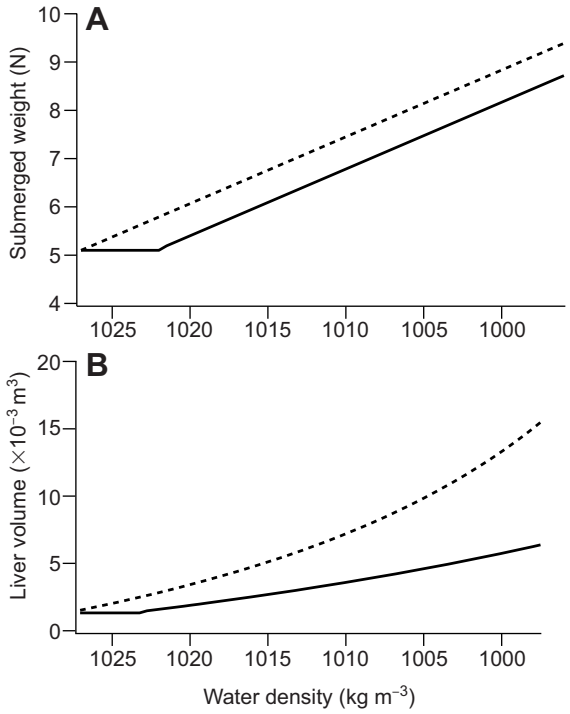

Fig. 1. Modelled implications of water density for the buoyancy control of elasmobranchs. Data were modelled based on Eqn 1 and parameterized with a hypothetical shark of 15 kg with the same body composition and tissue densities as those observed in Baldridge (1970). The stippled line indicates the response to changing environmental density if no compensation in liver density occurs. The solid lines represents the same model, assuming that the animal has the ability to reduce its liver density to those encountered in neutrally buoyant deep-sea sharks (∼920 kg m^{-3}) representing the lowest liver densities encountered in elasmobranchs. (A) Assuming no morphological changes (i.e. constant tissue volumes and densities), submerged weight would increase by ∼120% for a shark moving into fresh water. A reduction in liver density to 920 kg m^{-3} would be able to compensate any changes in water density up to ∼1025 kg m^{-3}, yet still resulting in submerged weight doubling. (B) Negative buoyancy may also be compensated by changes in liver size; in order to maintain the same submerged weight (4.5 N) as in marine waters, our hypothetical shark's liver would have to increase 8-fold in volume (stippled line) and even if liver density were reduced, liver volume would have to increase 3- to 4-fold to maintain similar buoyancy as in marine waters. These cases would result in liver size comprising 70% or 35% of whole body volume respectively compared with 11% in marine waters. In all scenarios described, lean tissue density and volume are unchanged.

are based on two representative swim speeds, namely, the so-called minimum speed (u_{min}) used to minimize total drag (Eqn 5); and the optimal speed (u_{opt}) maximizing travel distance with a fixed energy store (Weihs, 1973). Teleosts and elasmobranchs also travel over long distances in a manner that reduces energy consumption. But biological organisms incur metabolic costs at u=0 (known as standard metabolic rate) resulting from the other energy intensive functions of the body; this cost demands that metabolic efficiency is achieved at higher velocities than u_{min} – hence the larger u_{opt}. Typically, sharks swim at average speeds in the range of 0.3 to 0.8 m s^{-1} (Watanabe et al., 2012) – presumably near optimal speed – which amounts to twice (or less) the minimal speed (as shown further here). Not surprisingly, both minimal and optimal speeds, and corresponding metabolic costs, increase with larger negative buoyancies (see Eqns 6A and 6B). This trend will be shown quantitatively here using u_{min} since it can be assessed with a minimum of assumptions. Given that the calculation of u_{opt} involves several inputs characteristic of metabolism, which predictably vary

The Journal of Experimental Biology (2015) 218, 1099-1110 doi:10.1242/jeb.114868

Table 1. Hypothetical morphological scenarios modelled in response to changing salinity

	Scenario 0	Scenario 1	Scenario 2	Scenario 3	Scenario 4
	Marine	No compensation	Increasing liver size	Decreasing liver density	Increasing liver size and decreasing liver density
Mass (kg)	14.5	14.5	18.3	14.5	18.3
Water density (kg m^{-3})	1026	996	996	996	996
Lean tissue density (kg m^{-3})	1076	1076	1076	1076	1076
Liver tissue density (kg m^{-3})	964	964	964	920	920
Lean tissue volume (m^3)	0.0118	0.0118	0.0118	0.0118	0.0118
Liver tissue volume (m^3)	0.0020	0.0020	0.0045	0.0021	0.0045
Surface area of body (m^2)	0.59	0.59	0.66	0.59	0. 66
Fineness (*t*/SL)	0.212	0.212	0.234	0.211	0.234
Projected frontal area (m^2)	0.035	0.035	0.045	0.035	0.045
Submerged weight (N)	4.40	8.44	7.26	7.47	4.44

Scenario 0 represents the null model of the morphological characters for a 1.25 m bull shark in marine waters.

between species and encountered temperature, the dependence of optimal speed and metabolic expenditure shall be shown algebraically rather than numerically (see Eqns 6B, 20–27 below). Note finally that other optimized swimming speed concepts have been proposed (e.g. Castro-Santos, 2006; Videler and Nolet, 1990; Ware, 1978). Although optimizing different metrics, most, if not all, should show similar trends with regards to adding more negative buoyancy because of the increasing mechanical cost associated with a given speed.

We simulated four hypothetical scenarios that could be a response to changing water density; no compensation, increasing liver size, decreasing liver density and the two combined. These four scenarios markedly differed in the parameters used in our modelling exercise (Table 1) and resulted in an increase of negative buoyancy compared with marine waters. The scenarios do not encompass all possible morphological adaptations, such as body and fin profiles to improve lift (of which evolution into a ray-like lifting body profile would be one example). They aim instead at evaluating the effects of liver density and size modifications separately from those leading specifically to lift enhancement. Although the latter was not considered here, it should be clear from the modelling that, despite possible reductions in parasitic drag, lift increase always come at a cost, either in extra induced drag and/or loss of turn rate performance in unsteady maneuvering. All scenarios resulted in an increase of negative buoyancy compared with marine waters. We found a marked increase of the speed at which drag is minimized, primarily as a result of the increased negative buoyancy of those scenarios (Fig. 2).

An increase in liver size and a decreasing liver density resulted in the smallest increase of either cost of transport or metabolic power at minimum cost speed (u_{min}), but also resulted in less streamlining, with lower body depth over body length ratio (*t*/SL) and body wetted area both increased by 13% (Fig. 3). Our numerical work to solve u_{opt} also showed that optimal speed is dependent on buoyancy and mechanical power requirements increase with increasing negative buoyancy (see the Materials and methods). Namely, both u_{opt} and P_{total} increase with negative buoyancy (W) as $u_{opt} \propto W^0$ and $u_{opt} \propto W^{1/2}$ at small and large negative buoyancy, respectively, which, interestingly, compares with u_{min} as $u_{min} \propto W^{1/2}$ (Eqn 5); and $P^{opt}_{total} \propto W^0$ and $P^{opt}_{total} \propto W$, again at small and large W.

Densities of freshwater elasmobranchs

All sawfish (N=17) and bull sharks (N=5) captured in the Fitzroy River were negatively buoyant in the water they were captured in, with calculated body densities of 1065±5 kg m^{-3} for the bull sharks and 1065±3 kg m^{-3} for the sawfish. The ratio of W_{sub} and weight in air W_{air} (mass×9.81 m s^{-2}) was 6.44±0.39% in bull sharks and 6.48±0.33% in sawfish (Table 2). For the individuals where liver size and density could be measured, the liver represented 6.21±0.64% of whole body mass in the sawfish (N=2) and 7.82 ±1.73% in the bull shark (N=3). Liver density was 980±2 kg m^{-3} in the sawfish and 920±3 kg m^{-3} in the bull sharks (Table 3).

Comparative data

Comparisons of the ratio between weight in air and submerged weight shows that the 22 individuals of the two species we studied show some of the greatest negative buoyancies (6.4%), compared with the 113 individuals sampled in other studies in marine waters (3.95±1.2%, see supplementary material Table S1). Our statistical model of mass and submerged weight supports this, with the most parsimonious model indicating that habitat and mass are the strongest predictors of submerged weight (Table 4, Fig. 4). The

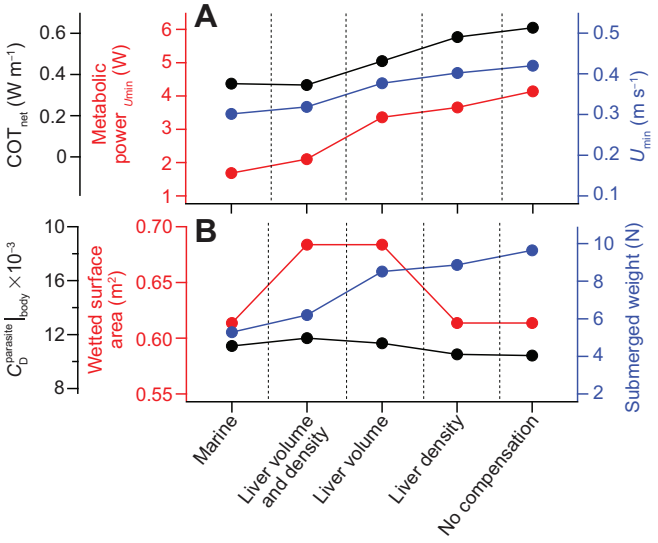

Fig. 2. Parameters and results of our modelling exercise for a bull shark of 1.2 m standard length. (A) All scenarios result in increasing costs of locomotion, as a result of increasing u_{min} which increases drag. All hypothetical scenarios also result in increasing cost of transport, with the exception of the scenario where liver size increases and liver density decreases. (B) This pattern is a result of all scenarios being characteristic of increased negative buoyancy, with the lowest increase where both density and size have been altered. Based on our considerations of u_{min}, all potential compensatory strategies result in increased costs. Based on u_{min}, increases in liver size and liver density should be the optimal strategy for compensation. This, however, ignores the cost of swimming at faster speeds, which is discussed in Fig. 3.

The Journal of Experimental Biology (2015) 218, 1099-1110 doi:10.1242/jeb.114868

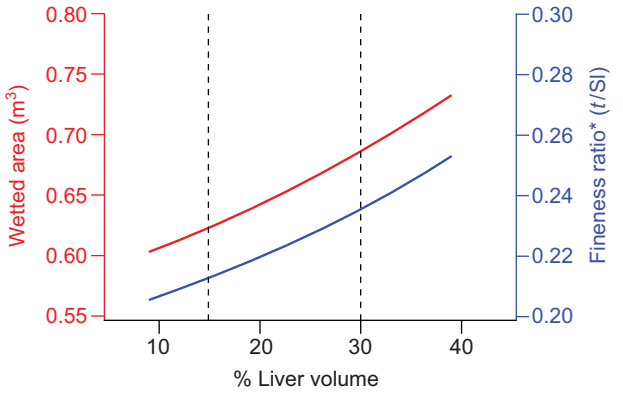

Fig. 3. Hydrodynamics of increasing liver size. To gauge the costs associated with faster speeds that may be employed during foraging, we model the implications of increasing liver sizes on drag. As induced drag responds $1/u^2$, its contribution to total drag at greater speeds will diminish, whereas parasite drag will increase u^2. Here, we show that increasing liver size results in an increase of two of the primary parameters that contribute to parasite drag. Drag is proportional to wetted area (Eqn 3) and our approximation suggests that this parameter will increase by >10% from liver volume of 15–30% (dashed vertical lines). The fineness ratio is the dominant factor in the calculation of $C_D^{parasite}|_{body}$ (Eqn 3). Increasing the fineness ratio by 10% subsequently results in a less streamlined body and a higher drag coefficient proportional to that increase. These data therefore suggest that compensatory mechanisms involving increasing liver size may reduce the costs at low swimming speeds, but will result in significantly increased costs at faster speeds. Note that our definition of 'fineness ratio' is the inverse of its typical use. We have chosen to adhere to this format as a result of the formulation in Eqn 3.

comparison of liver size scaling between elasmobranchs sampled in marine waters from previous research and those sampled in freshwater revealed that there was little difference in the size of livers, with the highest ranked model only including log mass as an explanatory factor. Lifestyle did not appear to affect liver size in our data-set; this, however, is a result of excluding deep-water sharks, which are known to have large livers, from our analysis (Bone and Roberts, 1969; Corner et al., 1969). Liver density, by contrast, is best predicted by the inclusion of lifestyle and habitat. Pelagic sharks have livers of lesser density than those species that are generally associated with the seabed. The five individuals for which livers could be sampled showed that liver densities that were below or near the lower 95th percentile of individuals of similar lifestyle sampled in marine waters (Fig. 4). Density of lean tissue was not predicted well by any of the covariates we tested the model for (Table 4).

DISCUSSION

Our comparison of body composition of sharks sampled in marine waters and those in freshwater suggest that liver size has not drastically increased to produce more upthrust and compensate for the lower density of freshwater. Liver density, by contrast, was measured to be close to the lowest values observed in any species of shark, suggesting that this may be a response to reduced water density. We emphasize that these conclusions do not stem from experimental data of how liver size and density responded to changing salinity in a controlled experiment, but rather a large comparative analysis of liver sizes and densities of a range of species. However, we can safely say that no substantial increase in liver size appears to have occurred in the individuals we studied. The same caveat also applies to our assessment of liver density; but in this case, the liver densities were lower than the 95th percentile of those studied to date, indicating that liver density may be readily lowered. There is precedence for such a process in the literature – experimentally weighted spiny dogfish (*Squalus acanthias*) increase their fraction of DAGE (a low density lipid) in liver tissue (Malins and Barone, 1970). Although not explicitly quantified in their study, a greater amount of DAGE will increase the upthrust provided by the liver and compensate for the increased negative buoyancy. No change in liver size was found in the experimentally weighted spiny dogfish.

Our analysis makes one important assumption: all lean tissue is fixed in its volume. A reduction in the volume of dense tissue (e.g. muscle, viscera, skeleton), would reduce any increases in surface area and therefore the energetic consequences we outline here. However, any reduction in the volume of these tissues must invariably decrease some form of performance. For instance, a reduction of white muscle volume (the most voluminous tissue in most fish) would be expected to lead to a proportional decline in

Table 2. Details of all sawfish and bull sharks that were weighed in air and while submerged

	Specimen	TL (mm)	Mass (g)	W_{sub} (N)	Buoyancy ratio (%)	V (ml)	P_{Shark} (kg m^{-3})
Carcharhinus leucas	1	862	4175	2.50	6.11	3936	1060.8
	2	824	3390	2.35	7.08	3163	1071.9
	3	851	4145	2.60	6.39	3896	1064.0
	4	950	4815	2.89	6.13	4538	1061.0
	5	840	3765	2.40	6.51	3534	1065.3
Pristis pristis	1	1224	4600	2.74	6.07	4338	1060.3
	2	1018	2365	1.47	6.34	2224	1063.4
	3	1140	3780	2.48	6.69	3541	1067.4
	4	1151	3660	2.26	6.28	3444	1062.8
	5	1090	3130	1.91	6.23	2947	1062.2
	6	1082	2890	1.81	6.40	2716	1064.1
	7	1025	3015	1.81	6.14	2841	1061.1
	8	1119	3060	2.01	6.70	2866	1067.5
	9	1021	2170	1.32	6.22	2043	1062.1
	10	1207	4230	2.75	6.62	3966	1066.6
	11	1079	2765	1.77	6.51	2595	1065.4
	12	1040	2760	1.96	7.25	2570	1073.8
	13	1104	2895	1.91	6.74	2711	1067.9
	14	1025	2215	1.47	6.77	2073	1068.3
	15	912	1530	1.03	6.86	1431	1069.4
	16	1172	4000	2.50	6.38	3760	1063.8
	17	1120	3600	2.11	5.97	3399	1059.3

The Journal of Experimental Biology (2015) 218, 1099-1110 doi:10.1242/jeb.114868

Table 3. Details of the sawfish (*n*=2) and bull sharks (*n*=3) that were available for full necropsies

	Carcharhinus leucas				*Pristis pristis*		
	1	2	3	Mean±s.d.	1	2	Mean±s.d.
Total length (mm)	862	824	851	846±20	1146	1130	1138±11
Mass (g)	4175	3390	4145	3903±445	4000	3600	3800±283
W_{sub} (N)	2.50	2.35	2.60	253±13	2.50	2.07	235±28
Body volume (ml)	4429	3634	4410	4158±454	4255	3813	4034±312
Mass/submerged weight (%)	6.11	7.08	6.39	6.53±0.50	6.38	5.97	6.17±0.28
Mass excluding liver (g)	3860	3150	3750	3587±382	3770	3360	3565±290
Submerged weight excluding liver (g)	280	225	260	255±28	255	215	235±28
Liver mass (g)	410	226	289	308±93	230	240	235±7
Liver volume (ml)	450	235	320	335±108	234	245	240±8
Body volume excluding liver (ml)	3594	2937	3504	3345±356	4021	3579	3800±312
Body density (kg m^{-3})	1061	1072	1064	1066±6	1064	1059	1060±3
Body density excluding liver (kg m^{-3})	1074	1073	1070	1072±2	1068	1064	1066±3
Liver volume (%)	7.71	6.22	8.88	7.60±1.33	5.51	6.15	5.83±0.45
Liver mass (%)	9.81	6.65	6.98	7.82±1.74	5.75	6.67	6.21±0.65
Liver density (kg m^{-3})	910	960	904	920±31	982	980	981±2

burst swimming performance. A simple example, for a shark to maintain similar hydrodynamic characteristics (fineness ratio, buoyancy, wetted area, Table 1) the liver would have to occupy ∼45% of the whole fish, reducing lean tissue volume by >50% in freshwater. Assuming white muscle comprises 40–70% of the animal's volume (Bone, 1978; Greek-Walker and Pull, 1975), this would result in a 76–100% reduction in available white muscle for burst swimming, with obvious deleterious effects to fitness (Ghalambor et al., 2003; Walker et al., 2005). Even though it may be possible to maintain similar hydrodynamic properties, compensation by reduction of volume of other tissue should have additional deleterious effects.

Optimal compensation – a paradox?

Our field data indicate that the reduction of liver density is the prevalent mechanism by which sharks achieve more upthrust. Yet our modelling approach suggests that in addition to decreasing liver density, increasing liver size to 30% body volume (scenario 4) provides a more-efficient alternative in our hypothetical shark (see Fig. 2), because of the reduced negative buoyancy. However, increasing liver size will increase body fineness ratio (t/SL) and thus wetted area (by ∼13%), as well as parasitic drag force (by >25%, see Eqns 2 and 3); but interestingly, it would also decrease u_{min} (by ∼18%; see Eqn 5) and overall COT (Fig. 2) compared with the scenario lacking compensation. However, less streamlining by increased liver volume would also degrade the performance of burst swimming as well as of foraging at supra-optimal speeds since, with $u>u_{min}$, the resulting drag force would become even higher and to the point of increasing COT, perhaps at levels too high for the given fixed amount of muscle power and energy available. In other words, combining lower liver densities with larger liver volumes could only be advantageous in environments where prey is easy to find and catch (at u_{min}) and predation pressure is low.

An additional explanation for this discrepancy is the metabolic cost of growing and maintaining such large livers. The low-density lipids contained in the liver responsible for providing upthrust are energy dense. For instance, triacylglycerols, a class of lipid found in shark livers (Wetherbee and Nichols, 2000), contain 38 kJ g^{-1}, whereas muscle tissue contains approximately 2–4 kJ g^{-1}. This may make a substantial difference for the juvenile sharks studied here, which are in a period of rapid somatic growth. Indeed, Priede et al. (2006) have suggested that the metabolic cost associated with large livers may be responsible for the absence of sharks from the oligotrophic abyssal depths of the oceans. Moreover, liver tissue has some of the fastest turnover time of any tissue in elasmobranchs (Hussey et al., 2010), therefore increasing the cost of not only growing but also maintaining such tissue. Although it may be argued that ∼30% liver volume is encountered in deep-sea sharks and some very large pelagics (e.g. basking, tiger or white sharks) and is therefore unlikely to provide an overwhelming metabolic burden, the warm tropical waters occupied by our study subjects already significantly increase standard metabolic rates (Carlson and Parsons, 1999). The increasing metabolic cost of growing a large liver may therefore not be sustainable for juvenile elasmobranchs in tropical waters.

Ecological implications

Activity represents an important component of the energy balance of most fish (Boisclair and Leggett, 1989) and our results indicate that greater negative buoyancies will result in increased costs, as shown by our modelled increases in u_{min} and u_{opt}. Such behavioral modification will increase the energetic cost of locomotion because such power costs increase with swimming speed at exponents of 2–3 (Alexander, 2003; Lowe, 2001). Our results confirmed that despite some compensation by liver density, the negative buoyancies of the two species we studied are approximately twice as great as those of a typical marine elasmobranch of similar mass and lifestyle. At u_{min} the power required to swim is approximately doubled compared to marine water. At u_{opt}, by contrast, the power would be expected to increase by as much, if not more, depending on the value of GW^2/β. The increased activity costs will depend on a variety of species-specific factors including the ecology of the species, typical swimming speeds, and the amount of time spent resting on the bottom.

Evolutionary implications

Increasing costs of locomotion associated with freshwater residency itself does not preclude elasmobranchs from occupying freshwater habitats, but it may act as a constraint. Teleost fish often compete for the same ecological space with elasmobranchs, but the utility of a gas bladder as a source of upthrust largely negates the buoyancy problem faced by sharks and rays. Juvenile coho salmon (*Oncorhynchus kisutch*) collected along a salinity gradient display compensation in swim-bladder volume; in marine waters a bladder comprising 5% of whole body volume is adequate to provide near neutral buoyancy and in freshwater this volume only increases to 7%

The Journal of Experimental Biology (2015) 218, 1099-1110 doi:10.1242/jeb.114868

Table 4. Model selection criteria for three analyses comparing morphological data from freshwater elasmobranchs sampled as part of this study and marine forms published in previous papers

	Model	d.f.	log Lik	AICc	delta	Weight
Mass vs liver mass	log Liver mass~log mass	4	45.88	–83.4	0	0.433
	log Liver mass~log mass+lifestyle	6	47.21	–82.3	1.14	0.245
	log Liver mass~log mass+lifestyle+habitat	5	46.179	–81.8	1.6	0.194
	log Liver mass~log mass+habitat	7	48.002	–81	2.44	0.128
Mass vs W_{sub}	log W_{sub}~log mass+habitat	5	122.817	–233.9	0	0.5
	log W_{sub}~log mass+lifestyle+habitat+log mass×lifestyle	6	122.92	–231.7	2.18	0.168
	log W_{sub}~log mass+lifestyle	4	123.057	231.2	2.67	0.131
	log W_{sub}~log mass+habitat×lifestyle	7	119.679	231.1	2.86	0.12
Liver density	ρ_{liver}~lifestyle+habitat	6	254.169	–495.6	0	0.865
	ρ_{liver}~lifestyle	5	251.078	–491.6	3.96	0.120
	ρ_{liver}~habitat	4	247.401	–486.4	9.13	0.009
	ρ_{liver}~1	1	245.926	–485.6	9.94	0.006
Lean tissue density	$\rho_{lean\ tissue}$ ~1	1	77.389	–148.6	0	0.605
	$\rho_{lean\ tissue}$ ~habitat	4	77.415	–146.5	2.08	0.214
	$\rho_{lean\ tissue}$ ~lifestyle	5	78.033	145.6	3.01	0.135
	$\rho_{lean\ tissue}$ ~lifestyle+habitat	6	78.059	–143.4	5.16	0.046

Data from this study (see Fig. 2) and Baldridge, 1970 and Bone and Roberts, 1969.

(Weitkamp, 2008). This difference is unlikely to affect parasite drag, because surface area and fineness ratio will remain largely unchanged (Alexander, 1966). Indeed, the extraordinarily low density of air (~5 kg m^{-3} at 10 m depth at 25°C) compared with that of lipid (~900 kg m^{-3}), results in water density not having a great effect on upthrust provided in fish using gas-filled bladders. This suggests that elasmobranchs (and by extension all fish that utilize lipid only to provide upthrust) are disadvantaged in freshwater over those using gas.

Paleontological records also show that early elasmobranchs were not always scarce in freshwater, but dominated marine and freshwater environments by the late Devonian, ~400 million years ago, whereas ray-finned fishes only evolved into efficient swimmers in the Mesozoic, approximately 200 million years ago (Long, 1995). We therefore argue that the innovations by modern teleosts, the gas-bladder and its role in buoyancy control in particular, have resulted in a competitive edge over elasmobranchs and contributed to the contemporary low abundance and diversity of freshwater sharks and rays. The material constraints of tissues providing lift in elasmobranchs will inevitably result in greater negative buoyancies in freshwater and result in lower locomotory performance compared with those groups able to use gas. This effect can be somewhat offset; however, it appears that sharks are unable to escape the constraints of lipid-produced upthrust.

The patterns of diversity in freshwater elasmobranchs also supports our conclusions; ~76–84% of all elasmobranchs known to occupy freshwater are part of the order Myliobatiformes (Ballantyne and Fraser, 2013; Martin, 2005). Myliobatiforms are a group of

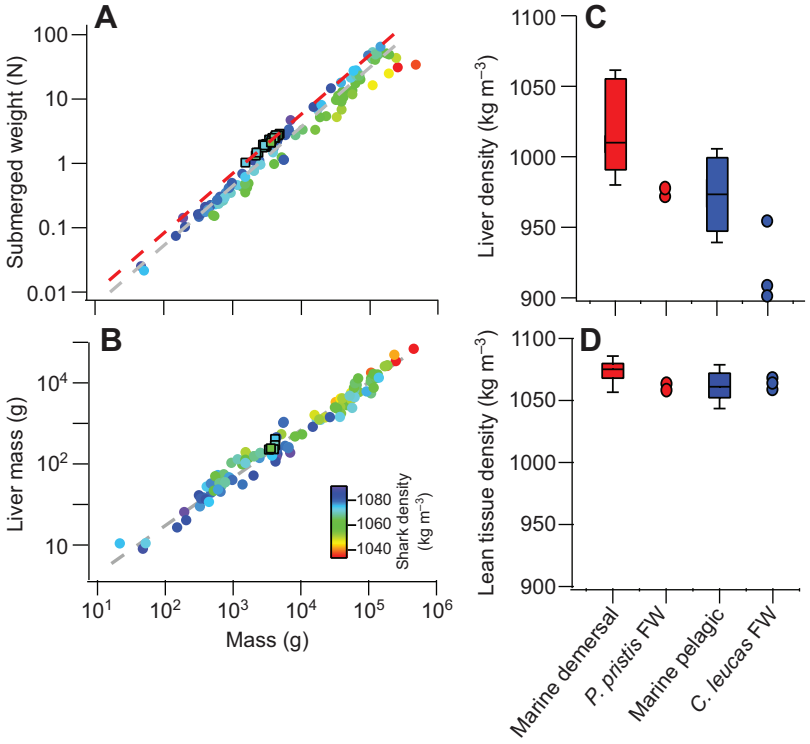

Fig. 4. Morphological differences in marine and freshwater elasmobranchs. (A) Significant differences were found in the submerged weight between all individuals sampled by Bone and Roberts (1969) and Baldridge (1970) in marine waters (gray dashed line, excluding species that are neutrally buoyant, such as deep-sea sharks and the basking shark *Cetorhinus maximus*) and *Carcharhinus leucas* (*N*=5) and *Pristis pristis* (*N*=20) sampled in freshwater as part of this study (red dashed line). (B) No differences in liver size between individuals sampled in marine environments and the two sawfish and three bull sharks that were available for full necropsy. (C) Comparison of liver density in the sharks sampled from marine waters and those from freshwater. The lifestyle of the species has a significant effect on liver density, with demersal individuals having denser livers than those that are pelagic. The two species we sampled in freshwater were close or below the lower 90th percentile for all marine individuals sampled previously suggesting that individuals occupying freshwater may have lower liver densities. (D) No major differences in lean tissue density could be detected between either lifestyles or habitat. See Table 4 for the model selection for all three analyses.

The Journal of Experimental Biology (2015) 218, 1099-1110 doi:10.1242/jeb.114868

largely benthic rays, such as whiprays (*Himantura* spp.) and stingrays (*Dasyatis* spp.). Individuals within this group are largely confined to movement close to the substratum (with some exceptions) and often occur over flat sandy or muddy substrates. The costs of increased negative buoyancy would be drastically reduced in those species, as a result of benthic resting and because the majority of swimming is performed close to the substrate. Swimming close to the bottom reduces the induced drag by a lifting surface as a result of increased pressure forming on the ventral side of the lifting surface, known as the ground effect (Webb, 1988). Indeed, in gliding bird flight, the ground effect may be responsible for a 49% reduction of drag due to lift (Hainsworth, 1988). The generally higher density of liver tissue in benthic elasmobranchs supports this, because there is less of an energetic incentive to reduce submerged weight in this group.

Our paper is the first to demonstrate that the reduced density of freshwater represents a significant physical challenge for elasmobranch locomotion that manifests as greatly increased negative buoyancy. These results indicate that freshwater sharks partially compensate with lower density liver tissue, rather than increasing overall liver volume. Given these data, elasmobranchs in freshwater habitats experience significant negative buoyancy and can only compensate by generating more lift through forward locomotion. Such behavioral compensation will result in greater energy expenditure from increased drag and we argue that buoyancy may have been an important factor constraining the reinvasion of freshwater by sharks and their relatives that may act in concert with osmoregulatory challenges. Additional data on the organismal biology of elasmobranchs occupying salinity gradients, as well as paleontological records, will be necessary to test these competing, but not mutually exclusive, hypotheses.

MATERIALS AND METHODS

Modelling the morphological consequences of environmental density

The following section largely follows the arguments by Alexander (1990), who tested the optimal means of producing lift as a function of swimming speed. Our model is constrained to a single means of producing increased buoyant force (liver lipid), while considering the implications of changing density of the occupied medium. The primary source of increasing the buoyant force in elasmobranchs is the liver, which has lower density (~900–1000 kg m^{-3}) than the other tissues of a shark (~1070 kg m^{-3}), the ratio of liver tissue to non-liver tissue is a major determinant of the buoyancy of a shark. According to Archimedes:

$$W = [(V_{\text{lean}}\rho_{\text{lean}} + V_{\text{liver}}\rho_{\text{liver}}) - (V_{\text{lean}} + V_{\text{liver}})\rho_{\text{water}}]\,\boldsymbol{g}, \quad (1)$$

where W refers to the submerged weight (or negative buoyancy) and $\boldsymbol{g}$ to the acceleration of gravity (9.81 m s^{-2}). Moreover, V_{lean} and V_{liver} are the volume of lean and liver tissue, respectively, and ρ_{lean} and ρ_{liver} are their respective densities. Thus the overall volume and density of the shark are given by $V_{\text{shark}}=V_{\text{lean}}+V_{\text{liver}}$ and $\rho_{\text{shark}}=(V_{\text{lean}}\,\rho_{\text{lean}}+V_{\text{liver}}\,\rho_{\text{liver}})/V_{\text{shark}}$, respectively.

Here, we define lean tissue to be all tissue excluding the liver. This set of equations, in turn, permits us to estimate the physical consequences of changing water density, i.e. changing ρ_{water} to 996 kg m^{-3}, representing the density of freshwater at 28°C compared with 1026 kg m^{-3} of marine water on submerged weight and the liver size required to offset the reduced upthrust provided by the environment. These two phenomena were also investigated under the assumption that sharks could alter the density of their livers, which has been experimentally shown for *Squalus acanthias* (Malins and Barone, 1970). A low value for liver density was taken to be 920 kg m^{-3}, representing the livers of deep-sea sharks (Bone and Roberts, 1969; Corner et al., 1969) because these animals must face similar constraints in reducing their submerged weight, while presumably minimizing liver size.

Modelling the energetic consequences of changing water density

We investigated, from first principles, the energetic consequences of a hypothetical shark moving into freshwater, and considered a range of mechanisms that could be employed to compensate for the decreasing water density compared with the marine conditions. Changing buoyancy impacts the attendant metabolic expenditures given the changes in swimming speed, as well as in body lift and drag, which are required to maintain a level trajectory. Such changes are being assessed herein with the type of aerodynamic modelling that is common in aircraft design (Dole, 1981; Pope, 1951). The basics of this modelling, along with the most important results will be discussed in this section, and the mathematical details further explored below and in the Appendix.

Although the inclusion of low-density lipids in the liver reduces negative buoyancy, hydrostatic forces are not sufficient to achieve neutral buoyancy in most species. In elasmobranchs (and many other obligate swimmers) this is achieved through forward motion-generated lift, which, in turn, increases drag. Swimmers face two general (physical) energetic costs incurred by moving through their environment, namely, those related to parasite drag ($F_{\text{D}}^{\text{parasite}}$), as generated by the fluid's friction against the body, as well as from the low pressure of the wake turbulence behind the body; and to induced drag ($F_{\text{D}}^{\text{induced}}$), as created by the lift production arising from the upward-angling of the anterior portion of the body and pectoral fins, and also from the downward thrust component created by the asymmetric caudal tail. For leopard shark (*Triakis semifasciata*), the balance of lift production is estimated at approximately 45% from the pectoral fins and 55% from the caudal fin (Fish and Shannahan, 2000), and we note that these values represent the only estimates of the distribution of lifting forces resulting in dynamic equilibrium in sharks.

Parasite drag applied to a shark moving at speed u can be generally calculated as:

$$F_{\text{D}}^{\text{parasite}} = \frac{1}{2}\rho_{\text{water}}u^2 \cdot S_{\text{ref}} \cdot C_{\text{D}}^{\text{parasite}}. \quad (2)$$

S_{ref} is the reference surface area used when extracting the parasite drag coefficient ($C_{\text{D}}^{\text{parasite}}$) from experimental data (usually, by inverting Eqn 2). Here, S_{ref} is defined as the product of the precaudal length SL and the body maximum width WD (including pectoral fin span). However, the parasite drag coefficient is modelled as the sum of the parasite drag (i.e. friction plus pressure drag) arising separately from the body and from all fins: $C_{\text{D}}^{\text{parasite}}=C_{\text{D}}^{\text{parasite}}|_{\text{body}}+\sum C_{\text{D}}^{\text{parasite}}|_{\text{fins}}$ ($\sum$ symbolizes a sum over each fin's contribution). The body parasite drag ($C_{\text{D}}^{\text{parasite}}|_{\text{body}}$) is expressed in a form developed by Hoerner in his drag studies of bodies of revolution (Blevins, 1992):

$$C_{\text{D}}^{\text{parasite}}|_{\text{body}} = \frac{K}{Re^{\alpha}}\frac{\text{SA}}{S_{\text{ref}}}\left[1 + 1.5\left(\frac{t}{\text{SL}}\right)^{3/2} + 7.0\left(\frac{t}{\text{SL}}\right)^{3}\right]. \quad (3)$$

The parasite drag due to all fins can be expressed similarly, albeit in a more complicated form, and is further discussed below and in the Appendix (see Eqns 13, 15, 16, A1 and A2). Here, the effects of pressure drag are represented by the terms in t/SL, with t representing the body's maximum diameter without the fins and SL the pre-caudal length. The coefficient K/Re^{α} represents the effects of the fluid's shear stress on the body, with Re as the body's Reynolds number, Re=SL·u/ν, and with ν as the fluid's kinematic viscosity [(1.15×10^{-6} and 1.13×10^{-6} m^2 s^{-1} for sea water and fresh water (16°C), respectively)]. The fins' parasite drag coefficient likewise includes a similar friction factor. The coefficient K and exponent α (>0) parameterize the fluid's friction as the combined result of a shark's denticulated skin and swimming motions on the body (Oeffner and Lauder, 2012; Shelton et al., 2014). Recent studies of shark hydrodynamics make it clear that the interactions of the boundary layer generated by the skin's denticles interacts with the flows created by the tail's motions in ways that do not always minimize body drag, and moreover in ways that are difficult to quantify in simple formulas such as in Eqn 3 (Shelton et al., 2014). In the interest of

The Journal of Experimental Biology (2015) 218, 1099-1110 doi:10.1242/jeb.114868

simplicity, the values of K and α correspond to those of a smooth flat plate in longitudinal flow and supporting a turbulent boundary layer [K=0.072 and α=0.2 (Blevins, 1992)]. It should be stressed that using flat plate drag data should not be viewed as approximating shark skin as smooth; but rather as a proxy for translating the complex interactions between denticulated skin and tail motions, as suggested by the averaging of the few rigid body and active swimming drag data so far available on a single shark species (Anderson et al., 2001).

The total drag exerted on the body is calculated by adding induced drag to the parasite drag of Eqn 2. The former is derived from the fact that the induced drag coefficient is proportional to the square of the lift force (Dole, 1981) and is given by:

$$F_{\mathrm{D}}^{\mathrm{induced}} = \frac{(1+\delta)}{\pi \mathrm{AR}} \cdot \frac{(F_{\mathrm{lift}})^2}{\left(\frac{1}{2}\rho_{\mathrm{water}} u^2\right) \cdot \mathrm{SL} \cdot \mathrm{WD}}. \quad (4)$$

Parameter AR is an overall body aspect ratio, here defined as that of the body's maximum width, plus combined pectoral fin span, over pre-caudal body length SL (or AR=WD/SL). The force F_{lift} is the total lift generated by all parts of the body. Since it is assumed that the shark is swimming horizontally and at constant speed, lift thus equals negative buoyancy ($F_{\mathrm{lift}}=W$). Finally, δ is an aerodynamic efficiency factor that is set to zero (with aircraft, δ is typically less than 0.05).

Estimation of the metabolic expenditures connected to increased drag-production involves a metric of speed. Postponing the study of expenditures generated at the optimal speed (Weihs, 1973), we first consider metabolic expenditures incurred at speeds $u=u_{\mathrm{min}}$ where total drag is minimal (Alexander, 1990). As discussed further by Dole (1981), a point of minimum drag exists in cases where lift equals weight in aircraft (or body lift equals negative buoyancy in sharks), as parasite and induced drag are proportional to u^2 and $1/u^2$ respectively. Furthermore, u_{min} is also the point at which induced drag is equal to parasite drag. Thus, solving the latter constraint with Eqns 2 and 4 yields a way to calculate u_{min}:

$$(u_{\mathrm{min}})^4 = \frac{1}{1/2\rho_{\mathrm{water}} \cdot \mathrm{WD} \cdot \mathrm{SL} \cdot C_{\mathrm{D}}^{\mathrm{parasite}}} \cdot \frac{2W^2}{\pi(\mathrm{WD})^2 \rho_{\mathrm{water}}}. \quad (5)$$

Note that from Eqns 3, 14, 15, A1 and A2, it follows that $C_{\mathrm{D}}^{\mathrm{parasite}}$ is also proportional to $(1/u_{\mathrm{min}})^{\alpha}$, with α defined by Eqn 3, so that the final dependence on negative buoyancy will be as $u_{\mathrm{min}} \sim W^{1/(4-\alpha)}$ (or $\sim W^{1/3.8}$ using the flat plate proxy). This result, used along with Eqn 2, thus suggests that increasing negative buoyancy will indeed lead to higher swim speed and thus to higher drag.

The total metabolic power (P_{total}) required for a shark to move its body through the water at u_{min} will be given by:

$$P_{\mathrm{total}} = \frac{1.5F_{\mathrm{D}}^{\mathrm{total}}}{\eta} u_{\mathrm{min}} = \frac{1.5F_{\mathrm{thrust}} \cos\theta}{\eta} u_{\mathrm{min}}. \quad (6A)$$

The second equation highlights the fact that the thrust has a vertical component due to the lift produced by the heterocercal caudal fin. In cases where the latter $\sim 0.55W$ (Fish and Shannahan, 2000) the thrust's angle θ with respect to the horizontal would be calculated from $\tan\theta = 0.55W/F_{\mathrm{D}}^{\mathrm{total}}$. The factor 1.5× arises from those effects of lateral tail-beat undulations (which increase the required thrust) that remained unaccounted for by the proxy factor $K/Re^{0.2}$ above [this proxy averages friction drag of rigid and swimming scup and dogfish in Anderson et al. (2001)]. [In comparison, a factor of 2.5–3 fold has been used in fish as compared to a rigid model by Webb (1971b).] Finally, the factor η measures both metabolic and propulsive inefficiencies of the tail and body, and is set here to $\eta \sim 0.20$ (Webb, 1971a).

Being oriented perpendicularly to a shark's motion at all times means that the lift force used to compensate for negative buoyancy does not perform any mechanical work on the body. However, lift generation does involve metabolic energy production since lift production always incurs additional drag in comparison to an identical body generating no lift. This can be done by re-writing P_{total} as resulting from the power used to compensate for total drag, i.e. from the sum of parasite drag (Eqn 2) and induced drag (Eqn 4). As discussed further below (Eqns 17–21), and evaluated for any arbitrary speeds u, one has:

$$P_{\mathrm{total}} = \frac{1}{\eta_{\mathrm{sw}}} \left[\left(\frac{1}{2}\rho_{\mathrm{water}} \cdot S_{\mathrm{ref}} \cdot C_{\mathrm{D}}^{\mathrm{parasite}} u^3 \right) + \frac{(1+\delta)}{\pi(\mathrm{WD}/\mathrm{SL})} \frac{2W^2}{\rho_{\mathrm{water}}(\mathrm{WD} \cdot \mathrm{SL}) \cdot u} \right] + W_{\mathrm{m}}. \quad (6B)$$

Here η_{sw} is a speed-dependent function ($\eta_{\mathrm{sw}}=\beta u$) representing both metabolic and propulsive efficiency of the tail's propulsive apparatus, and the constant W_{m} the standard metabolic rate corresponding to the internal metabolic processes that are independent of speed during active swimming (Weihs, 1973). The second term in Eqn 6B is what distinguishes a fish swimming horizontally while neutrally buoyant ($C_{\mathrm{L}}=0$), and an elasmobranch doing the same but at $C_{\mathrm{L}} \neq 0$. With the latter and at minimum speed, this second term shows an explicit dependence on, and an increase with, negative buoyancy ($\sim W^2$).

The increased metabolic cost of swimming at the optimal speed (u_{opt}) while experiencing increased negative buoyancy can be assessed by using Eqn 6b along with the approach proposed by Weihs (1973). This is done by optimizing the distance travelled (l) at fixed stored energy ($E=P_{\mathrm{total}}\, l/u$), i.e. as a solution of the differential equation $\mathrm{d}l/\mathrm{d}u|_{\mathrm{opt}}=0$ under the constraint of lift-compensated negative buoyancy. As shown in Eqns 17–21, P_{total} would increase with negative buoyancy (W) as $P_{\mathrm{total}}^{\mathrm{opt}} = 2W_{\mathrm{m}} + 4GW^2/\beta u_{\mathrm{opt}}^2$ with $G=2(1+\delta)/(\pi \mathrm{AR} \cdot \rho_{\mathrm{water}} \cdot \mathrm{SL} \cdot \mathrm{WD})$. The optimal speed also increases with W, namely as $u_{\mathrm{opt}} \propto W^0$ and $u_{\mathrm{opt}} \propto \mathrm{W}^{1/2}$ at small and large negative buoyancy, respectively, after solving the algebraic equation $3GW^2/\beta = \left(\tau\beta u_{\mathrm{opt}}^4 - u_{\mathrm{opt}}^2 W_{\mathrm{m}}\right)$ where $\tau \equiv 1/2\rho_{\mathrm{water}} S_{\mathrm{ref}} C_{\mathrm{D}}^{\mathrm{parasite}}$. Here, the parameter GW^2/β determines the regime where the negative buoyancy can be considered as 'small' or 'large'. Using typical shark morphological inputs, this ratio is estimated at ~0.3–0.6 $W\ \mathrm{m}^2\ \mathrm{s}^{-2}$, which places sharks somewhere in between the two limits. With both β and W_{m} being unknown in sharks, a quantitative assessment of the increased costs associated with higher negative buoyancy is currently out of reach.

Eqns 2–6A,B and 21 now allow us to calculate a power–velocity relationship, i.e. where velocity=u_{min} and =u_{opt}, respectively, for hypothetical sharks in water of different densities. It has to be noted that these equations are not analogous to the metabolic rate–swimming speed relationships (where u is an independent variable), but rather are designed to provide the lowest hypothetical costs of swimming at a given water density even though no single shark can have an ideal pectoral fin (or body angling) to maximize lift-to-drag ratio over the range of speeds simulated. Indeed, some species will feature morphological adaptations for faster cruising whereas others will be adapted for slower speeds. We have also reflected this in our efficiency term η, which would be expected to vary with swimming speed of an individual, but here we will assume that the muscle geometry and tail-beat kinematics are, so that η is maximized at u_{min}, mimicking a fish adapted to the cruising speed that minimizes required power. Muscular efficiency has been experimentally determined for rainbow trout (*Onchorhynchus mykiss*) and showed that maximum efficiency achieved was 20% (Webb, 1971a).

Finally, to facilitate comparisons of the energetic impact of changing water density, we computed the net cost of transport ($\mathrm{COT}_{\mathrm{net}}$) to reflect the energetic cost of moving the animal (and its variable mass depending on liver size) 1 m in distance.

$$\mathrm{COT}_{\mathrm{net}} = \frac{P_{\mathrm{total}}}{m \times u_{\mathrm{min}}}. \quad (7)$$

With regards to the drag calculations, the necessary input morphometric data for the bull shark and smooth dogfish discussed in the sections below are listed in supplementary material Tables S2–S5.

We decided to model four hypothetical scenarios (see Table 1 for all parameters used in the models described previously) that sharks could use to counteract changing buoyancies.

Scenario 1 – no compensation

Elasmobranchs do not alter their morphology in response to changing environmental density and the mechanical costs of swimming change in accordance with the increasing negative buoyancy.

Scenario 2 – reducing liver density

Elasmobranchs have been shown to respond to experimentally increased negative buoyancy by decreasing the density of their livers (Malins and Barone, 1970), effectively increasing the buoyant force and reducing negative buoyancy. This scenario would result in no change in liver size (and no changes in surface area), but would dampen the increase in negative buoyancy with decreasing water density. We consider a liver density of 920 kg m^{-3} to be a lower bound of liver density. Livers of this density are encountered in neutrally buoyant sharks such as *Cetorhinus maximus* (Bone and Roberts, 1969).

Scenario 3 – increasing liver size

Increasing the size of the liver is another mechanism by which more upthrust can be generated and the impact of decreasing water density can be mitigated. We consider that the upper ceiling of hypothetical livers is when liver tissue constitutes 30% of body volume. This represents a realistic upper bound. Similar liver sizes are encountered in sharks that are close to neutral buoyancy and these species face a similar constraint in minimising negative buoyancy. Increasing liver volume while maintaining the volume of lean tissue is expected to increase surface area and decrease fineness ratio, affecting parasite drag.

Scenario 4 – increasing liver size and reducing liver density

This scenario represents a combination of scenarios 2 and 3. The two distinct processes can act synergistically in providing more buoyancy. We modelled the energetic consequences of these four scenarios, using the observed body composition of bull sharks (*Carcharhinus leucas*) captured in Florida by Baldridge (1970). Namely, we consider that the lean tissue density is 1075 kg m^{-3}, the nominal liver density is 964 kg m^{-3} and liver volume represents 11% of whole body volume. We parameterized this model with a shark of 1 m pre-caudal length and an associated mass of 15 kg (Thorburn, 2006).

Field methods

Animal capture

Largetooth sawfish (*Pristis pristis* Linnaeus 1758) and bull sharks (*Carcharhinus leucas* Müller and Henle 1839) were captured between September and October 2011 and 2012 in the Fitzroy River, Western Australia. Animals were captured using bottom-set gill nets (15 and 20 cm stretched mesh-size) set at night. Nets were checked at regular intervals of 1.5 h.

Measurement and calculation of body density

Captured sawfish and bull sharks were initially sexed and measured. Animals were weighed to the nearest 5 g using a sling and digital hanging-scale (UWE HS 7500 series, capacity: 7500 g, resolution: 5 g). To determine the submerged weight (W_{sub}) of the animals, a sling was suspended from a tripod (Daiwa infinity weigh tripod) in water of approximately 1.2 m depth. Before animals were placed into the sling, the weight of the sling was zeroed. Animals remained motionless in the sling and a weight was read after the scale stabilized. While weighing, it was ensured that no part of the sling touched the river-bed or the tripod. After submerged weight was determined, we measured the mass of animals using the same sling and scale, without submergence. Care was taken that no water remained in the sling when the mass was determined. Following these measurements, whole body density (ρ_{shark}) was calculated based on the density of fresh water at 28°C, the common water temperature during night time (A.C.G. and D.L.M., unpublished data) with a corresponding water density of 996 kg m^{-3}, as determined by the relation: $\rho_{shark}=(W_{air}\ \rho_{water})/(W_{air}-W_{sub})$.

Determination of liver density and liver-free body density

All individuals that perished in gill nets were used for further analysis of buoyancy regulation. After determining whole body density, fish were dissected and liver density and volume was determined by displacing livers in a graded water cylinder. Livers were forcefully submerged with a long toothpick, to overcome positive buoyancy. The volume of the toothpick was negligible in relation to liver volume. Liver density (ρ_{liver}) was simply calculated from mass and displaced volume. Density of the liver-free body (ρ_{lean}) was determined in the same fashion as prior to dissection of the liver, by determination of mass and submerged weight using the described sling.

Meta-analysis of densities in marine and freshwater elasmobranchs

In order to compare buoyancy between marine and freshwater forms, we collated all such measurements from the literature, primarily based on two publications (Baldridge, 1970; Bone and Roberts, 1969). Some parameters were not reported in these original papers (e.g. liver-free density), but could be calculated based on the data provided. We excluded any deep-sea individuals from the analysis due to significantly different densities (near neutral) as a result of the different lifestyle, as well as the basking shark for the same reason, resulting in 113 individuals of 27 marine species being included in the analysis. In order to compare our data from freshwater elasmobranchs to the marine forms, we analyzed the data using mixed models, because of unbalanced sample size for the different species (Zuur et al., 2007). To account for these repeated measures on a single species, we used the species ID as a random effect in our model. Models also included lifestyle as a covariate, which was determined based on the species description in Compagno (2001), separating species into two groups considered to exclusively associate with the sea-bed (demersal) and those that swim in the water column (pelagic and bentho-pelagic, see supplementary material Table S1), as previous papers have shown the impact of lifestyle on buoyancy in elasmobranchs (Bone and Roberts, 1969). Mixed models were fitted using the 'lme4' plug in implemented in the R statistical package (R Development Core Team, 2010) and model selection was based on small sample corrected Akaike's information criterion (AIC_c) computed in the model selection package 'MuMin'.

Calculation of the wetted area SA

We calculated the reference area for skin friction, represented by the wetted skin surface area (SA), from volume (V) and girth (G) based on the empirically determined relationship between surface area and standard length (SL) and girth for 10 species of galeoid shark by Musick et al. (1990), which can be expressed as:

$$\mathrm{SA} = 0.71(G \times \mathrm{SL}). \tag{8}$$

Girth can be calculated from volume, assuming that the shape of the animal is similar to that of two paraboloids (P_1 and P_2) joined at their base, where P_1=1/3 SL and P_2=2/3 SL, assuming fusiform shape.

$$V = 0.5\pi\ \frac{1}{3}\mathrm{SL}\ h^2 + 0.5\pi\ \frac{2}{3}\mathrm{SL}\ h^2. \tag{9}$$

Parameter h refers to the radius of the base circle of each paraboloid, i.e. the radius of the body section where maximum girth would be measured. Solving Eqn 9 for h results in:

$$h = \sqrt{\frac{V}{0.5\pi\left(\frac{1}{3}\mathrm{SL} + \frac{2}{3}\mathrm{SL}\right)}}. \tag{10}$$

From h, girth can be calculated using the following equation, assuming a circular cross-section:

$$G = 2\pi\ h. \tag{11}$$

Combining Eqns 8, 10 and 11 results in the equation used to calculate surface area as a reference area for the skin friction drag (Eqn 2):

$$\mathrm{SA} = 0.71\left(2\pi\ \mathrm{SL}\sqrt{\frac{V}{0.5\pi\left(\frac{1}{3}\mathrm{SL} + \frac{2}{3}\mathrm{SL}\right)}}\right). \tag{12}$$

The Journal of Experimental Biology (2015) 218, 1099-1110 doi:10.1242/jeb.114868

We have to note here that the circular cross-section is an approximation only, because many species of sharks only have a quasi-circular cross-sectional area and this varies between species and the axial location of the cross-section. We selected this approach for its simplicity and generality.

Fin parasite drag coefficient (all fins but caudal)

In aircraft design, a wing's drag is calculated with computer programs such as XFOIL which, from an airfoil's known shape and dimension data, yields the parasite and induced drag, the lift force, aerodynamic moments, etc. (Drela, 1989). Having no information about the airfoil profiles of the fins, and again given the uncertainties connected with the hydrodynamic effects of the denticular skin and body motions on the boundary layer, we resort to a simpler approach which, as we indicate below, yields results that are in reasonable agreement with shark experimental data.

The parasite drag force corresponding to each one of the caudal and non-caudal fin is calculated from Eqn 2, with a drag coefficient similar to Eqn 3, also developed by Hoerner while studying the pressure drag on symmetrical airfoils (Blevins, 1992; p. 352):

$$C_{\mathrm{D}}^{\mathrm{parasite}}|_{\mathrm{fin}} = \frac{\mathrm{SA}}{S_{\mathrm{ref}}} C_{\mathrm{friction}}^{\mathrm{fin}} \left[1 + 2.0\left(\left\langle \frac{t_{\mathrm{fin}}}{\mathrm{FC}} \right\rangle\right) + 60.0\left(\left\langle \frac{t_{\mathrm{fin}}}{\mathrm{FC}} \right\rangle\right)^4\right]. \quad (13)$$

The terms in $\langle t_{\mathrm{fin}}/\mathrm{FC}\rangle$ represent the mean fin maximum thickness over fin chord, as averaged over chord span. Herein $\langle t_{\mathrm{fin}}/\mathrm{FC}\rangle$=0.2 for all caudal and non-caudal fins. The factor $C_{\mathrm{friction}}^{\mathrm{fin}}$ corresponds to the friction created by the fluid's shear stress on each side of a given fin. This coefficient is calculated by first approximating a fin as a right triangle as shown in supplementary material Fig. S1A,B. Secondly, and under an assumption of no cross-flows along the span FS (or in other words, with flows above and below each fin moving strictly chord-wise) the net shear stress (friction) applied to the fin is seen as equivalent to adding the shear stress sustained by narrow rectangular strips (of skin) covering both sides of the fin (supplementary material Fig. S1B,C). Using the same proxy drag per span length and per dynamic pressure on a rectangular plate, K/Re^{α}, each strip thus sustains a friction force equal to:

$$\delta F_{\mathrm{friction}}^{\mathrm{strip}} = \frac{1}{2}\rho_{\mathrm{water}} u^2 \cdot X \cdot \Delta \cdot \frac{K}{(uX/\nu)^{\alpha}}. \quad (14)$$

Note that with airfoils, there is a sum of two factors of the form K/Re^{α}, reflecting the fact that a strip's (airfoil's) boundary layer changes from laminar to turbulent (Pope, 1951). Such transition points change span-wise, especially on tapered wings, but such information is unavailable for shark fins. Once more, a simpler and more conservative approach is to use the flat plate proxy with K=0.072 and α=0.2 all over the strip (assuming a turbulent boundary layer). Returning to Eqn 14, it should be noted that the force $\delta F_{\mathrm{friction}}^{\mathrm{strip}}$ is very small if the strip width Δ is small. In fact, the planform fin area and the superposition of the strips on one side of the fin is one of the same if the latter is infinitesimal. Thus after replacing Δ with dy and strip length x by y (FC/FS) (the x–y right triangle and FC–FS right triangle having the same tangent, or height-over-base ratio), Eqn 14 can be integrated exactly over the fin span FS and yield the actual friction drag force sustained by the fin. Using SA as reference area, the fin friction drag coefficient thus becomes:

$$C_{\mathrm{friction}}^{\text{non-caudal fin}} = \left(\frac{\frac{1}{2}\mathrm{FC}\cdot\mathrm{FS}}{\mathrm{SA}}\right)\cdot 2 \cdot \frac{K_{\mathrm{fin}}}{(u_{\mathrm{min}}/\nu)^{\alpha}}\left(\frac{\mathrm{FC}}{\mathrm{FS}}\right)^{1-\alpha}\left(\frac{1}{2-\alpha}\right)\left(\frac{(\mathrm{FS})^{2-\alpha}}{\frac{1}{2}\mathrm{FC}\cdot\mathrm{FS}}\right). \quad (15)$$

The first factor in parentheses arises from the need to measure the drag coefficient with SA (per Eqn 3) rather than with 1/2 FC×FS, which is the 'natural' reference area of the strip-based calculation above. The factor '2' that follows is a consequence of the friction being exerted on both sides of the fin. The parasite drag force of a fin is then calculated by multiplying the friction drag coefficient above by the factor $1/2\,\rho_{\mathrm{water}}\,u^2$ SA, per Eqns 2 and 3.

Fin parasite drag coefficient (caudal only)

The calculation of the caudal fins' parasite drag is also based on Eqns 2, 13 and 14, but with a few modifications. With the caudal fins being swept triangles rather than right triangles, one needs an alternate construction in which two right triangles are embedded (supplementary material Fig. S2). Here, the friction coefficient of a swept fin section is calculated from the strips of length XA covering the swept section only, again as shown in supplementary material Fig. S2. The strip's drag is then calculated with Eqn 14, but with the factor X replaced by XA. Once more, Δ=dy. The integration is carried out exactly once two key geometric identities are used. First, and with respect to the (span-wise) distance y from the tip of a strip of length x=XA+XB overlapping the larger 'primary' right triangle (supplementary material Fig. S2), one has x/y=(FCA+FCB)/FS. Secondly, from the strip section of length x' spanning the smaller 'secondary' right triangle only, there is x'/y=*FCB*/*FS*. Here x'=x−XA and thus x/y=(FCB/FS)+(XA/y). Equating both identities yields XA=(FCA/FS)y, from which the integration is carried exactly. The result is:

$$C_{\mathrm{friction}}^{\mathrm{caudal fin}} = \left(\frac{\frac{1}{2}\mathrm{FCA}\cdot\mathrm{FS}}{\mathrm{SA}}\right)\cdot 2 \cdot \frac{K_{\mathrm{fin}}}{(u_{\mathrm{min}}/\nu)^{\alpha}}\cdot\left(\frac{\mathrm{FCA}}{\mathrm{FS}}\right)^{1-\alpha}\cdot\left(\frac{1}{2-\alpha}\right)\cdot \left(\frac{(\mathrm{FS})^{2-\alpha}}{\frac{1}{2}\mathrm{FCA}\cdot\mathrm{FS}}\right). \quad (16)$$

The data used to calculate drag for both the bull shark and smooth dogfish are listed in supplementary material Tables S2–S5.

Validation of the drag model

The drag and COT modelling described herein was validated with the shear stress drag data of smooth dogfish (*Mustelus canis*) measured by Anderson et al. (2001). The pressure drag contributions in Eqns 3 and 13 were shut-off by multiplying by zero the pressure drag terms in t/SL and t_{fin}/FC, respectively. Typically, the model calculates pressure drag contributing as much as 15–20% of the total drag on the smooth dogfish. Anderson et al. measured shear stresses on *M. canis* both during swimming and in a 'rigid body' mode in a 20 cm s^{-1} flow tank (Re=9×10^4), obtaining friction coefficients of 0.0146 and 0.0076, respectively. The model for a dogfish with the same dimensions yields an overall friction coefficient of 0.0116 (fins and body combined), as calculated at u_{min}=18.8 cm s^{-1} and Re=8.5×10^4. This result is very close to the average of Anderson et al.'s active swimming and rigid body data, which should not be surprising since the shear stress factor K/Re^{α} used in Eqns 3 and A2 (with K=0.072 and α=0.2) tracks very well the Anderson et al. scup and dogfish data in the range $10^4<Re<10^5$.

Validity of the overall model

We have assumed that lean tissue density and volume is not adjusted in response to changing water density. Even if such adjustments were to take place in nature, such a process would clearly reduce performance of the individual in several aspects. For instance, if white muscle mass was reduced to allow for larger livers in an effort to maintain streamlining, the capacity for burst swimming for either predator escape or prey capture would be reduced. Presumably, having very watery muscle tissue also reduces performance (Pelster, 2009).

As discussed briefly in the Appendix, our parasitic drag model is insensitive to angle of attack, as long that is, either pectoral fins or body are inclined at angles away from stall angles of attack. Generally, postural data for sharks actively swimming in the water column have shown that at usual cruising speeds, body angles are near horizontal (Fish and Shannahan, 2000). Note also that our model considers that the vortex jet of the caudal fin will have a vertical component, although in reality this may change with swimming speed (Wilga and Lauder, 2002).

Although we could attempt to model the lift produced by the flattened ventral surface at significant angle of attacks, previous studies and first principles suggest that this may be not an effective strategy to offset the mechanical challenges associated with freshwater residency in sharks and rays. Treating the body as a lifting surface would require different lift and drag coefficients than those used because a shark's body would be worse at

generating lift (and better at producing drag) compared with a cambered hydrofoil. An extreme example: the experimental amputation of *M. canis* pectoral fins caused a negative head pitching moment, which, in turn, was behaviorally compensated for by swimming at an angle 45 deg above horizontal (Fish and Shannahan, 2000). This suggests that for this shark species the body alone at a pitch angle of 45 deg generates the same lift as the pectoral fins at 8–10 deg angle of attack. Because the pectoral fins essentially balance the moment generated by a heterocercal caudal fin (Fish and Shannahan, 2000), this type of extreme modification of behavior could significantly increase the amount of lift generated during swimming. However, this degree of body pitch during steady swimming is not realistic for efficient locomotion because of the increase in drag from excessive projected area parallel to the animal's trajectory. Nevertheless, in the absence of lift generated by either pectoral fins or liver density, a tilted body during swimming could produce lift to counter sinking (Aleyev, 1977). This seems to be used when sharks are swimming very slowly and thus are not producing enough lift from either control or propulsive surfaces, presumably at the cost of increased drag (Fish and Shannahan, 2000). All these effects would exacerbate the dramatic increase in costs associated with low speed travel shown here (Fig. 4C). A shark in trim effectively minimizes the area of the body exposed to flow thereby reducing drag, even despite the induced drag generated by the lift-producing pectoral fins (Fish and Shannahan, 2000).

The metabolic costs of negative buoyancy compensation when swimming at optimal speed (u_{opt})

The fish modelling used by Weihs (1973) assumed neutral buoyancy as would be in the case of a teleost fish with a gas bladder, and as such may not apply to fish with negative buoyancy compensated by lift. Generally, lift generation involves extra metabolic expenditures because it always incurs additional drag. This was shown earlier with the speed at minimum drag (u_{in}), and proved here in the case of the optimal speed using Weihs' approach.

While swimming at any speed u, the total metabolic power (P_{total}) expended is mostly used to overcome total drag, i.e. parasite drag (Eqn 2) and induced drag (Eqn 4):

$$P_{total}=\frac{1}{\eta_{sw}}\left[\left(\frac{1}{2}\rho_{water}\cdot S_{ref}\cdot C_D^{parasite}u^3\right)+\frac{(1+\delta)}{\pi(WD/SL)}\frac{2W^2}{\rho_{water}(WD\cdot SL)\cdot u}\right]+W_m. \quad (17)$$

In the above, the lift force has already been set equal to the negative buoyancy (W). Also, the standard metabolic rate W_m corresponds to those metabolic processes deemed as independent of swimming speed (Weihs, 1973). Finally, the coefficient η_{sw} corresponds to metabolic and propulsive efficiency of the body–tail apparatus. In what follows, and along with Weihs (1973), this efficiency factor is considered to be speed dependent:

$$\eta_{sw}=\beta u, \quad (18)$$

with β being a constant specific to the species under consideration. Note that η_{sw} is different from η used in Eqn 6A. Following Weihs (1973), the total energy E stored in sharks, as well as their speed u and distance travelled l, are related as follows:

$$E=(P_{tail}+W_m)\frac{l}{u}, \quad (19)$$

where $P_{tail}=P_{total}-W_m$ (P_{tail} corresponds to W_p in Weihs, 1973). The optimal speed u_{opt} is now defined as the speed that maximizes the distance travelled (l) at fixed stored energy (E), i.e. as a solution of the differential equation $dl/du|_{opt}=0$ under the constraint of lift-compensated negative buoyancy. For neutrally buoyant teleosts (where $W=0$), Weihs showed the optimal speed was given by $u_{opt}^2=\beta W_m/(1/2\ \rho_{water}\ S_{ref}\ C_D^{parasite})$ and the corresponding metabolic expenditures by $P_{total}^{opt}=2W_m$ (Weihs, 1973). For a lift-producing shark, however, the optimization procedure yields

$$\frac{3GW^2}{\beta}=\left(\frac{\tau}{\beta}u_{opt}^2-W_m\right)\cdot u_{opt}^2, \quad (20)$$

which determines the value of the optimal speed; and the corresponding metabolic expenditures:

$$P_{total}^{opt}=2W_m+4\frac{GW^2}{\beta u_{opt}^2}. \quad (21)$$

To simplify the notation in the equations above, parameters τ and G have been defined as:

$$\tau\equiv\frac{1}{2}\rho_{water}\cdot S_{ref}\cdot C_D^{parasite}, \quad (22)$$

$$G\equiv\frac{(1+\delta)}{\pi(WD/SL)}\cdot\frac{2}{\rho_{water}\cdot WD\cdot SL}. \quad (23)$$

Solving the latter exactly is carried out by changing variables (i.e. setting $z=u_{opt}^2$) and solving a quadratic equation. The result is rather complicated, however, with a sum of square roots embedded within another square root. A calculation in specific limits is instead more informative. At small values of the negative buoyancy (W) where the term in G can be neglected in Eqn 20:

$$u_{opt}=\sqrt{\frac{\beta W_m}{\tau}}, \quad (24)$$

$$P_{total}^{opt}=2W_m. \quad (25)$$

At large values of negative buoyancy where G and u_{opt} are very large in Eqn 20:

$$u_{opt}=\left(\frac{3G}{\tau}\right)^{1/4}W^{1/2}, \quad (26)$$

$$P_{total}^{opt}=2W_m+\frac{4G}{\beta}\cdot\sqrt{\frac{\tau}{3G}}\cdot W. \quad (27)$$

From these results, one obtains $u_{opt}\propto W^0$ and $u_{opt}\propto W^{1/2}$ at small and large negative buoyancy respectively; and $P_{total}^{opt}\propto W^0$ and $P_{total}^{opt}\propto W$ again at small and large W. Here, the parameter GW^2/β determines the regime where the negative buoyancy can be considered as 'small' or 'large'. To see which limit is more relevant to sharks, the value of GW^2/β is calculated as follows.

As the exact value of the proportionality constant β and standard metabolic rate W_m are either unknown or can vary substantially with circumstance for sharks, a rough estimate is used instead, by using in Eqn 18 the value $\eta_{sw}\sim\eta\sim0.2$ and $u_{opt}\sim0.6$ m s^{-1} (per the averaged shark data discussed in Watanabe et al., 2012). One obtains $\beta\sim1/3$, which along with typical shark morphological inputs and values of negative buoyancy ~6 N (marine scenario in Fig. 2; bull shark), yields $4GW^2/\beta u_{opt}$ in the range of 4 Watts. An estimate for W_m is obtained, by contrast, by comparing the latter with eight times the total metabolic power calculated via Eqn 6A (as $u_{opt}\sim2u_{min}$ and power$\sim u^3$), a comparison that suggests standard metabolic outputs of $W_m\sim8.0$ Watts at u_{opt}. Given that in Fig. 2 the negative buoyancies vary from 6 to 10 N, one would expect the term $4GW^2/\beta u_{opt}$ in Eqn 21 to grow by 4 times. And so these estimates suggest sharks to be somewhere in between the two limits highlighted by Eqns 24–27.

Acknowledgements

We would like to thank Yuuki Watanabe and two anonymous referees for their critical comments; they greatly increased the quality of our paper. Invaluable field support was provided by the Nyikina-Mangala Rangers. J.P. thanks G. Bramesfeld for fruitful discussions with regards to estimating the shear stress sustained by triangular flat surfaces.

Competing interests

The authors declare no competing or financial interests.

Author contributions

A.C.G., D.L.M. and J.A.G. conceived the study. A.C.G., J.J.K., J.M.W. and D.L.M. performed the fieldwork. A.C.G. and J.P. led the data-analysis with contributions

from J.A.G. A.C.G., J.P. and J.A.G. drafted the paper with contributions from all other authors.

Funding
This project was generously supported by grants from the Australia Pacific Science Foundation, National Geographic's Waitt Foundation Program, the Fisheries Society of the British Isles and the Western Australian Government's NRM program. A.C.G. was supported by an Endeavour Research Fellowship.

Supplementary material
Supplementary material available online at
http://jeb.biologists.org/lookup/suppl/doi:10.1242/jeb.114868/-/DC1

References

Aleyev, Y. G. (1977). *Nekton*. The Hague: Springer.
Alexander, R. M. (1966). Physical aspects of swimbladder function. *Biol. Rev.* **41**, 141-176.
Alexander, R. M. N. (1990). Size, speed and buoyancy adaptations in aquatic animals. *Am. Zool.* **30**, 189-196.
Alexander, R. M. N. (2003). *Principles of Animal Locomotion*. Princeton: Princeton University Press.
Anderson, E. J., McGillis, W. R. and Grosenbaugh, M. A. (2001). The boundary layer of swimming fish. *J. Exp. Biol.* **204**, 81-102.
Baldridge, H. D., Jr. (1970). Sinking factors and average densities of Florida sharks as functions of liver buoyancy. *Copeia* **1970**, 744-754.
Ballantyne, J. S. and Fraser, D. I. (2013). Euryhaline elasmobranchs. In *Fish Physiology: Euryhaline Fishes: Fish Physiology*, Vol. 32 (ed. S. D. McCormick, A. P. Farrell and C. J. Brauner), pp. 125-198. Oxford: Academic Press.
Ballantyne, J. S. and Robinson, J. W. (2010). Freshwater elasmobranchs: a review of their physiology and biochemistry. *J. Comp. Physiol. B Biochem. Syst. Environ. Physiol.* **180**, 475-493.
Blevins, R. D. (1992). *Applied Fluid Dynamics Handbook*. Malabar, FL: Krieger Publishing Company.
Boisclair, D. and Leggett, W. C. (1989). The importance of activity in bioenergetics models applied to actively foraging fishes. *Can. J. Fish. Aquat. Sci.* **46**, 1859-1867.
Bone, Q. (1978). Locomotor muscle. In *Fish Physiology*, Vol. 7 (ed. W. S. Hoar and D. J. Randall), pp. 361-424. New York: Academic Press.
Bone, Q. and Roberts, B. L. (1969). The density of elasmobranchs. *J. Mar. Biol. Assoc. UK* **49**, 913-937.
Carlson, J. K. and Parsons, G. R. (1999). Seasonal differences in routine oxygen consumption rates of the bonnethead shark. *J. Fish Biol.* **55**, 876-879.
Castro, J. I. (2011). *The Sharks of North America*. New York: Oxford University Press.
Castro-Santos, T. (2006). Modeling the effect of varying swim speeds on fish passage through velocity barriers. *Trans. Am. Fish. Soc.* **135**, 1230-1237.
Compagno, L. J. V. (2001). *Sharks of The World: An Annotated and Illustrated Catalogue of Shark Species Known to Date*. Rome: FAO.
Corner, E. D. S., Denton, E. J. and Forster, G. R. (1969). On the buoyancy of some deep-sea sharks. *Proc. R. Soc. B Biol. Sci.* **171**, 415-429.
Davenport, J. (1999). Swimbladder volume and body density in an armoured benthic fish, the streaked gurnard. *J. Fish Biol.* **55**, 527-534.
Dole, C. E. (1981). *Flight Theory and Aerodynamics*. New York: John Wiley & Sons.
Drela, M. (1989). XFOIL: an analysis and design system for low Reynolds number airfoils. In *Low Reynolds Number Aerodynamics* (ed. T. J. Mueller). pp. 1-12. Berlin: Springer.
Fish, F. E. and Shannahan, L. D. (2000). The role of the pectoral fins in body trim of sharks. *J. Fish Biol.* **56**, 1062-1073.
Ghalambor, C. K., Walker, J. A. and Reznick, D. N. (2003). Multi-trait selection, adaptation, and constraints on the evolution of burst swimming performance. *Integr. Comp. Biol.* **43**, 431-438.
Gleiss, A. C., Jorgensen, S. J., Liebsch, N., Sala, J. E., Norman, B., Hays, G. C., Quintana, F., Grundy, E., Campagna, C. and Trites, A. W. (2011a). Convergent evolution in locomotory patterns of flying and swimming animals. *Nat. Commun.* **2**, 352.
Gleiss, A. C., Norman, B. and Wilson, R. P. (2011b). Moved by that sinking feeling: variable diving geometry underlies movement strategies in whale sharks. *Funct. Ecol.* **25**, 595-607.
Greek-Walker, M. and Pull, G. A. (1975). A survey of red and white muscle in marine fish. *J. Fish Biol.* **7**, 295-300.
Hainsworth, F. R. (1988). Induced drag savings from ground effect and formation flight in brown pelicans. *J. Exp. Biol.* **135**, 431-444.
Hussey, N. E., Brush, J., McCarthy, I. D. and Fisk, A. T. (2010). δ15N and δ13C diet-tissue discrimination factors for large sharks under semi-controlled conditions. *Comp. Biochem. Physiol. A Mol. Integr. Physiol.* **155**, 445-453.
Lee, C. E. and Bell, M. A. (1999). Causes and consequences of recent freshwater invasions by saltwater animals. *Trends Ecol. Evol.* **14**, 284-288.
Long, J. A. (1995). *The Rise of Fishes: 500 Million Years of Evolution*. Baltimore: Johns Hopkins University Press.
Lowe, C. G. (2001). Metabolic rates of juvenile scalloped hammerhead sharks (Sphyrna lewini). *Mar. Biol.* **139**, 447-453.
Malins, D. C. and Barone, A. (1970). Glyceryl ether metabolism: regulation of buoyancy in dogfish *Squalus acanthias*. *Science* **167**, 79-80.
Martin, R. A. (2005). Conservation of freshwater and euryhaline elasmobranchs: a review. *J. Mar. Biol. Assoc. UK* **85**, 1049-1073.
Meloni, C. J., Cech, J. J., Jr, Katzman, S. M. and Gatten, R., Jr. (2002). Effect of brackish salinities on oxygen consumption of bat rays (Myliobatis californica). *Copeia* **2002**, 462-465.
Musick, J. A., Tabit, C. R. and Evans, D. A. (1990). Body surface area in galeoid sharks. *Copeia* **4**, 1130-1133.
Oeffner, J. and Lauder, G. V. (2012). The hydrodynamic function of shark skin and two biomimetic applications. *J. Exp. Biol.* **215**, 785-795.
Pelster, B. (2009). Buoyancy control in aquatic vertebrates. In *Cardio-Respiratory Control in Vertebrates* (ed. M. L. Glass and S. C. Wood), pp. 65-98. Berlin: Springer.
Pillans, R. D. and Franklin, C. E. (2004). Plasma osmolyte concentrations and rectal gland mass of bull sharks *Carcharhinus leucas*, captured along a salinity gradient. *Comp. Biochem. Physiol. A Mol. Integr. Physiol.* **138**, 363-371.
Pope, A. (1951). *Basic Wing and Airfoil Theory*. New York: reprinted by Dover Publications.
Priede, I. G., Froese, R., Bailey, D. M., Bergstad, O. A., Collins, M. A., Dyb, J. E., Henriques, C., Jones, E. G. and King, N. (2006). The absence of sharks from abyssal regions of the world's oceans. *Proc. R. Soc. B Biol. Sci.* **273**, 1435-1441.
R Development Core Team. (2010). *R: A Language and Environment for Statistical Computing*. Vienna, Austria: R Foundation for Statistical Computing.
Shelton, R. M., Thornycroft, P. J. M. and Lauder, G. V. (2014). Undulatory locomotion of flexible foils as biomimetic models for understanding fish propulsion. *J. Exp. Biol.* **217**, 2110-2120.
Thorburn, D. C. (2006). Biology, ecology and trophic interactions of elasmobranchs and other fishes in riverine waters of Northern Australia. Ph.D., pp. 135. Murdoch: Murdoch University.<CQ3>
Thorson, T. B. (1962). Partitioning of body fluids in the Lake Nicaragua shark and three marine sharks. *Science* **138**, 688-690.
Vermeij, G. J. and Dudley, R. (2000). Why are there so few evolutionary transitions between aquatic and terrestrial ecosystems? *Biol. J. Linn. Soc.* **70**, 541-554.
Videler, J. J. and Nolet, B. A. (1990). Costs of swimming measured at optimum speed: scale effects, differences between swimming styles, taxonomic groups and submerged and surface swimming. *Comp. Biochem. Physiol. A Physiol.* **97**, 91-99.
Walker, J. A., Ghalambor, C. K., Griset, O. L., McKenney, D. and Reznick, D. N. (2005). Do faster starts increase the probability of evading predators? *Funct. Ecol.* **19**, 808-815.
Ware, D. M. (1978). Bioenergetics of pelagic fish: theoretical change in swimming speed and ration with body size. *J. Fish. Res. Board Can.* **35**, 220-228.
Watanabe, Y. Y., Lydersen, C., Fisk, A. T. and Kovacs, K. M. (2012). The slowest fish: swim speed and tail-beat frequency of Greenland sharks. *J. Exp. Mar. Biol. Ecol.* **426-427**, 5-11.
Webb, P. (1971a). The swimming energetics of trout II. Oxygen consumption and swimming efficiency. *J. Exp. Biol.* **55**, 521-540.
Webb, P. W. (1971b). The swimming energetics of trout I. Thrust and power output at cruising speeds. *J. Exp. Biol.* **55**, 489-520.
Webb, P. W. (1988). Simple physical principles and vertebrate aquatic locomotion. *Am. Zool.* **28**, 709-725.
Weihs, D. (1973). Optimal fish cruising speed. *Nature* **245**, 48-50.
Weitkamp, L. A. (2008). Buoyancy regulation by hatchery and wild coho salmon during the transition from freshwater to marine environments. *Trans. Am. Fish. Soc.* **137**, 860-868.
Wetherbee, B. M. and Nichols, P. D. (2000). Lipid composition of the liver oil of deep-sea sharks from the Chatham Rise, New Zealand. *Comp. Biochem. Physiol. B Biochem. Mol. Biol.* **125**, 511-521.
Wilga, C. and Lauder, G. (2002). Function of the heterocercal tail in sharks: quantitative wake dynamics during steady horizontal swimming and vertical maneuvering. *J. Exp. Biol.* **205**, 2365-2374.
Zuur, A. F., Ieno, E. N. and Smith, G. M. (2007). *Analysing Ecological Data*. New York: Springer.

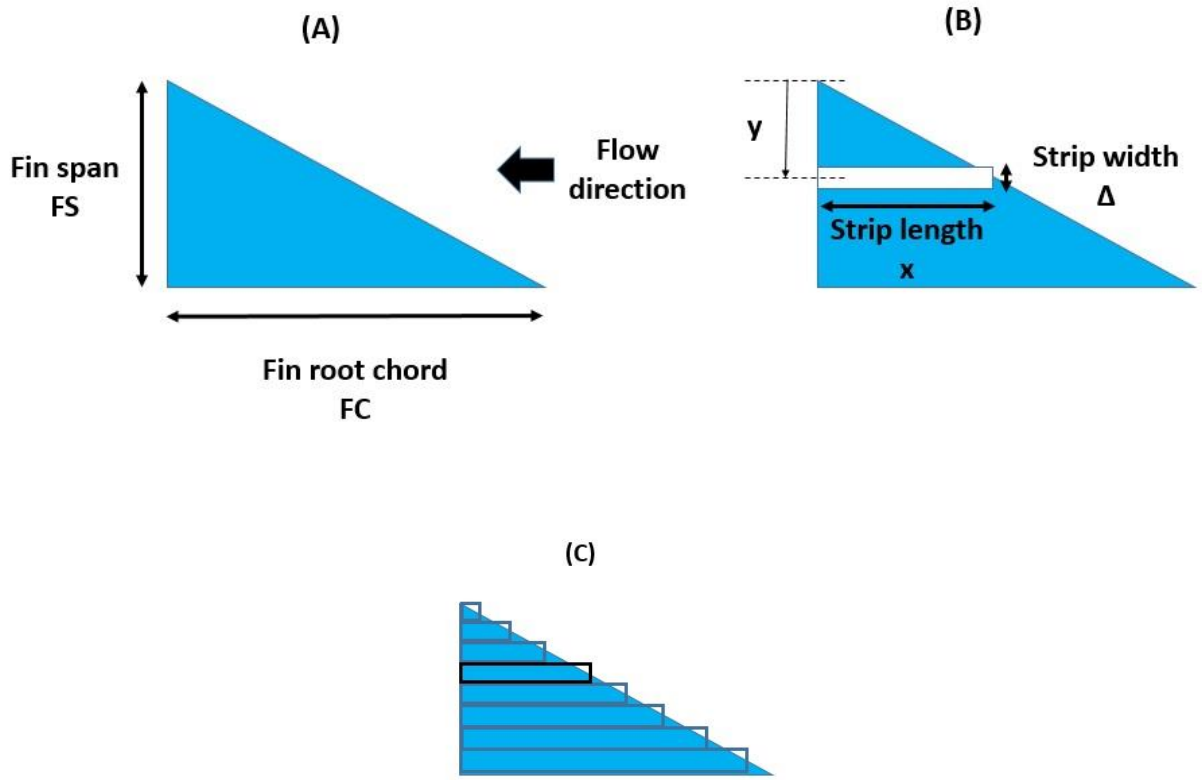

Fig. S1. Modelling non-caudal fins with right triangles. (A) basic geometry; (B) strip positioning and definition; (C) covering both sides of a fin with strips for shear stress integration.

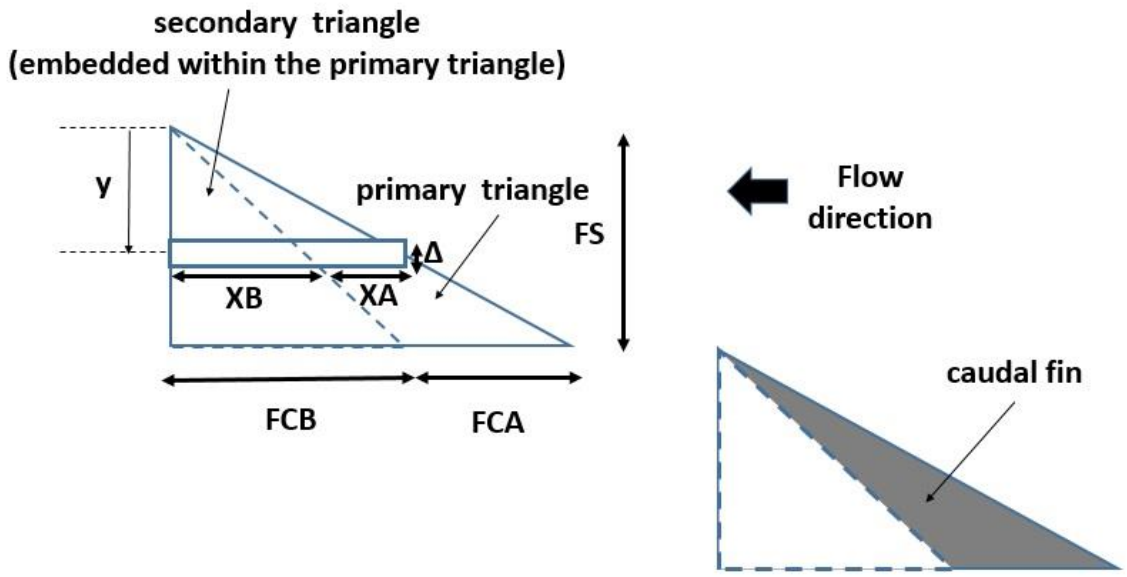

Fig. S2. Modelling caudal fins with right triangles. Top left: basic triangle ans strip dimensions; bottom right: location of the swept fin.

Table S1. Data on the body composition and density for all marine elasmobranchs, excluding deep-sea sharks and basking sharks studied by by Bone and Roberts (1970) and Baldridge Jr (1970) in marine waters used in the analysis of liver scaling and density according to lifestyle and habitat.

Species	Life Style	Mass (g)	Submerged Weight (g)	Wsub /Mass *100	Liver Mass	% Liver mass	Whole Animal Volume (ml)	Liver Volume (ml)	% Liver Volume	Liver Density (kg/m^3)	Whole Animal Density (kg/m^3)	Lean Tissue Density (kg/m^3)
Squalus Acanthias	bentho-pelagic	1,545.00	43.00	2.78	141.30	9.10	1,463.22	145.74	9.96	969.55	1,055.89	1,065.44
Squalus Acanthias	bentho-pelagic	1,627.00	43.00	2.64	161.80	10.00	1,543.11	166.49	10.79	971.84	1,054.37	1,064.35
Squalus Acanthias	bentho-pelagic	4,017.00	100.00	2.49	252.60	6.30	3,815.88	249.88	6.55	1,010.89	1,052.71	1,055.64
Squalus Acanthias	bentho-pelagic	1,707.00	50.00	2.93	142.00	8.30	1,614.22	144.86	8.97	980.25	1,057.47	1,065.09
Squalus Acanthias	bentho-pelagic	5,152.00	127.00	2.47	540.70	10.50	4,895.28	562.88	11.50	960.59	1,052.44	1,064.38
Squalus Acanthias	bentho-pelagic	1,362.00	44.50	3.27	97.90	7.20	1,283.49	100.54	7.83	973.78	1,061.17	1,068.60
Squalus Acanthias	bentho-pelagic	1,528.00	36.00	2.36	194.10	12.70	1,453.48	202.14	13.91	960.21	1,051.27	1,065.98
Scyliorhinus canicula	demersal	323.80	15.00	4.63	8.90	2.80	300.83	8.63	2.87	1,031.13	1,076.36	1,077.70
Scyliorhinus canicula	demersal	789.00	35.50	4.50	49.20	6.20	734.05	48.70	6.63	1,010.28	1,074.86	1,079.45
Scyliorhinus canicula	demersal	594.70	27.00	4.55	52.90	8.90	553.04	54.12	9.79	977.53	1,075.32	1,085.93
Scyliorhinus canicula	demersal	366.50	17.50	4.78	14.80	4.00	339.99	14.61	4.30	1,012.81	1,077.97	1,080.90
Scyliorhinus canicula	demersal	314.10	16.50	5.25	16.90	5.40	289.92	16.59	5.72	1,018.66	1,083.41	1,087.34
Scyliorhinus canicula	demersal	334.70	16.50	4.93	14.00	4.20	309.99	14.03	4.53	997.99	1,079.73	1,083.60
Scyliorhinus canicula	demersal	649.50	30.00	4.62	35.40	5.50	603.51	35.86	5.94	987.18	1,076.21	1,081.83

Scyliorhinus canicula	demersal	476.10	23.00	4.84	19.40	4.10	441.40	19.22	4.35	1,009.33	1,078.61	1,081.76
Scyliorhinus canicula	demersal	408.30	18.00	4.41	27.70	6.80	380.22	27.96	7.35	990.73	1,073.84	1,080.44
Scyliorhinus canicula	demersal	559.60	23.50	4.20	28.80	5.20	522.26	29.32	5.61	982.17	1,071.50	1,076.81
Scyliorhinus canicula	demersal	469.00	22.00	4.70	32.80	7.00	435.46	33.02	7.58	993.19	1,077.02	1,083.90
Scyliorhinus canicula	demersal	397.40	21.50	5.41	13.40	3.40	366.20	13.06	3.57	1,025.73	1,085.21	1,087.41
Scyliorhinus canicula	demersal	942.10	35.50	3.77	106.00	11.30	883.20	108.41	12.27	977.79	1,066.69	1,079.13
Scyliorhinus canicula	demersal	672.80	26.00	3.87	28.70	4.30	630.10	29.09	4.62	986.62	1,067.76	1,071.69
Scyliorhinus canicula	demersal	439.80	19.50	4.43	11.50	2.60	409.45	11.51	2.81	998.71	1,074.12	1,076.31
Scyliorhinus canicula	demersal	729.50	27.00	3.71	55.30	7.60	684.36	56.63	8.27	976.53	1,065.95	1,074.02
Scyliorhinus canicula	demersal	1,167.00	47.00	4.03	130.40	12.00	1,091.09	133.85	12.27	974.20	1,069.58	1,082.91
Mustelus Asterias	bentho-pelagic	2,050.00	78.50	3.83	154.70	7.20	1,920.60	156.75	8.16	986.95	1,067.37	1,074.52
Mustelus Asterias	bentho-pelagic	2,520.00	98.00	3.89	186.20	7.40	2,359.47	190.65	8.08	976.67	1,068.03	1,076.07
Mustelus Asterias	bentho-pelagic	762.50	30.00	3.94	35.30	4.60	713.59	35.36	4.96	998.22	1,068.54	1,072.21
Mustelus Asterias	bentho-pelagic	599.00	27.50	4.59	23.50	3.90	556.75	22.99	4.13	1,022.15	1,075.89	1,078.21
Galeorhinus galeus	Pelagic	544.00	15.50	2.85	49.50	9.10	514.86	49.39	9.59	1,002.20	1,056.61	1,062.38
Galeorhinus galeus	Pelagic	17,160.00	710.00	4.14	1,232.00	7.20	16,025.33	1,216.85	7.59	1,012.45	1,070.80	1,075.60
Galeorhinus galeus	Pelagic	629.00	24.00	3.82	33.60	5.30	589.38	36.14	6.13	929.66	1,067.22	1,076.21
Galeorhinus galeus	Pelagic	1,520.00	49.00	3.22	126.90	8.40	1,433.02	128.11	8.94	990.59	1,060.69	1,067.58

Prionace glauca	Pelagic	10,442.00	342.00	3.28	535.80	5.10	9,839.26	520.21	5.29	1,029.96	1,061.26	1,063.01
Prionace glauca	Pelagic	8,172.00	280.00	3.43	475.80	5.80	7,688.26	468.78	6.10	1,014.98	1,062.92	1,066.03
Prionace glauca	Pelagic	32,574.00	535.00	1.64	3,350.00	10.30	31,211.89	3,436.53	11.01	974.82	1,043.64	1,052.16
Prionace glauca	Pelagic	15,900.00	340.00	2.14	1,615.00	10.20	15,158.30	1,641.50	10.83	983.86	1,048.93	1,056.83
Prionace glauca	Pelagic	38,045.00	930.00	2.44	3,156.00	8.30	36,156.84	3,172.92	8.78	994.67	1,052.22	1,057.76
Prionace glauca	Pelagic	38,363.00	700.00	1.83	4,102.00	10.70	36,690.70	4,151.97	11.32	987.96	1,045.58	1,052.93
Squatina squatina	demersal	6,946.00	480.00	6.91	190.30	2.80	6,299.07	179.83	2.85	1,058.20	1,102.70	1,104.01
Squatina squatina	demersal	4,510.00	235.00	5.21	176.80	3.90	4,164.64	175.63	4.22	1,006.69	1,082.93	1,086.28
Squatina squatina	demersal	14,950.00	770.00	5.15	824.00	5.50	13,813.93	815.73	5.91	1,010.13	1,082.24	1,086.77
Squatina squatina	demersal	653.60	31.00	4.74	20.60	3.20	606.53	19.51	3.22	1,055.71	1,077.61	1,078.34
Squatina squatina	demersal	4,350.00	260.00	5.98	148.50	3.40	3,984.41	140.19	3.52	1,059.31	1,091.75	1,092.94
Squatina squatina	demersal	4,227.00	229.00	5.42	114.40	2.70	3,894.79	107.86	2.77	1,060.62	1,085.30	1,086.00
Lamna nasus	Pelagic	19,520.00	830.00	4.25	1,218.00	6.20	18,207.50	1,191.98	6.55	1,021.83	1,072.09	1,075.61
Lamna nasus	Pelagic	47,800.00	1,332.00	2.79	2,820.00	5.90	45,268.39	2,811.50	6.21	1,003.02	1,055.92	1,059.43
Lamna nasus	Pelagic	38,100.00	933.50	2.45	2,557.00	6.70	36,207.01	2,559.18	7.07	999.15	1,052.28	1,056.32
Scyliorhinus stellaris	demersal	4,357.00	216.30	4.97	455.30	10.50	4,033.80	462.93	11.48	983.51	1,080.12	1,092.65
Scyliorhinus stellaris	demersal	46.70	2.57	5.51	0.81	1.70	42.99	0.80	1.86	1,013.98	1,086.28	1,087.65
Scyliorhinus stellaris	demersal	21.30	0.96	4.51	1.09	5.10	19.81	1.03	5.21	1,055.55	1,074.95	1,076.01

Dasyiatis pastinaca	demersal	518.70	15.90	3.07	21.80	4.20	489.82	21.70	4.43	1,004.84	1,058.96	1,061.47
Raja clavata	demersal	3,950.00	175.50	4.44	198.40	5.00	3,677.06	198.73	5.40	998.32	1,074.23	1,078.57
Raja clavata	demersal	4,313.00	260.00	6.03	249.00	5.80	3,948.37	245.90	6.23	1,012.59	1,092.35	1,097.65
Raja clavata	demersal	3,860.00	151.00	3.92	255.60	6.60	3,613.25	260.05	7.20	982.89	1,068.29	1,074.91
Raja clavata	demersal	190.60	14.50	7.61	6.50	3.40	171.55	6.26	3.65	1,037.67	1,111.02	1,113.80
Raja mantagui	demersal	2,446.00	113.50	4.64	139.70	5.70	2,272.28	139.48	6.14	1,001.55	1,076.45	1,081.35
Raja mantagui	demersal	149.50	7.63	5.10	2.70	1.80	138.21	2.55	1.85	1,057.84	1,081.71	1,082.16
Raja mantagui	demersal	202.60	10.50	5.18	4.10	2.00	187.14	3.86	2.06	1,062.25	1,082.61	1,083.04
Raja mantagui	demersal	51.40	2.20	4.28	1.10	2.10	47.93	1.04	2.17	1,055.28	1,072.40	1,072.78
R microcellata	demersal	5,860.00	280.00	4.78	279.30	4.80	5,435.95	277.16	5.10	1,007.74	1,078.01	1,081.78
Galeocerdo cuvier	Pelagic	39,100.00	1,320.00	3.38	1,760.00	4.50	37,082.70	1,760.00	4.75	1,000.00	1,054.40	1,057.11
Galeocerdo cuvier	Pelagic	22,900.00	553.00	2.41	1,406.50	6.14	21,811.60	1,450.00	6.65	970.00	1,049.90	1,055.59
Galeocerdo cuvier	Pelagic	18,600.00	531.00	2.85	1,243.62	6.69	17,677.25	1,260.00	7.13	987.00	1,052.20	1,057.20
Galeocerdo cuvier	Pelagic	34,200.00	1,150.00	3.36	2,330.46	6.81	32,282.42	2,420.00	7.50	963.00	1,059.40	1,067.21
Galeocerdo cuvier	Pelagic	55,200.00	1,390.00	2.52	3,906.98	7.08	52,516.41	4,130.00	7.86	946.00	1,051.10	1,060.07
Galeocerdo cuvier	Pelagic	31,700.00	986.00	3.11	2,472.57	7.80	29,965.03	2,490.00	8.31	993.00	1,057.90	1,063.78
Galeocerdo cuvier	Pelagic	71,900.00	2,060.00	2.87	5,934.48	8.25	68,209.85	6,260.00	9.18	948.00	1,054.10	1,064.82
Galeocerdo cuvier	Pelagic	40,800.00	1,090.00	2.67	4,144.98	10.16	38,801.71	4,260.00	10.98	973.00	1,051.50	1,061.18

Galeocerdo cuvier	Pelagic	55,000.00	1,210.00	2.20	5,638.68	10.25	52,495.94	6,210.00	11.83	908.00	1,047.70	1,066.44
Galeocerdo cuvier	Pelagic	251,200.00	3,170.00	1.26	34,431.70	13.71	248,221.34	38,300.00	15.43	899.00	1,012.00	1,032.62
Galeocerdo cuvier	Pelagic	186,900.00	2,550.00	1.36	26,077.50	13.95	179,849.88	28,500.00	15.85	915.00	1,039.20	1,062.59
Galeocerdo cuvier	Pelagic	460,300.00	3,500.00	0.76	69,541.50	15.11	447,110.25	77,700.00	17.38	895.00	1,029.50	1,057.79
Galeocerdo cuvier	Pelagic	108,400.00	1,670.00	1.54	17,743.90	16.37	104,290.94	19,100.00	18.31	929.00	1,039.40	1,064.15
Negaprion brevirostris	Pelagic	136,100.00	5,230.00	3.84	16,100.00	11.83	128,287.30	17,274.68	13.47	932.00	1,060.90	1,080.96
Negaprion brevirostris	Pelagic	108,500.00	5,460.00	5.03	5,490.00	5.06	101,734.65	5,573.60	5.48	985.00	1,066.50	1,071.22
Negaprion brevirostris	Pelagic	108,200.00	4,280.00	3.96	12,800.00	11.83	101,988.88	13,646.06	13.38	938.00	1,060.90	1,079.88
Negaprion brevirostris	Pelagic	93,000.00	4,870.00	5.24	6,170.00	6.63	86,495.54	6,407.06	7.41	963.00	1,075.20	1,084.18
Negaprion brevirostris	Pelagic	107,000.00	4,500.00	4.21	10,900.00	10.19	100,441.19	11,546.61	11.50	944.00	1,065.30	1,081.06
Carcharhinus plumbeus	Pelagic	61,200.00	2,560.00	4.18	6,490.00	10.60	57,265.84	6,774.53	11.83	958.00	1,068.70	1,083.55
Carcharhinus plumbeus	Pelagic	66,400.00	2,610.00	3.93	8,840.00	13.31	62,312.31	9,305.26	14.93	950.00	1,065.60	1,085.89
Carcharhinus plumbeus	Pelagic	62,100.00	2,850.00	4.59	4,400.00	7.09	57,923.70	4,512.82	7.79	975.00	1,072.10	1,080.30
Carcharhinus plumbeus	Pelagic	60,800.00	1,780.00	2.93	7,570.00	12.45	57,564.86	7,918.41	13.76	956.00	1,056.20	1,072.18
Carcharhinus plumbeus	Pelagic	52,200.00	2,190.00	4.20	4,810.00	9.21	48,771.37	4,979.30	10.21	966.00	1,070.30	1,082.16
Carcharhinus plumbeus	Pelagic	62,600.00	2,380.00	3.80	9,800.00	15.65	58,735.22	10,392.36	17.69	943.00	1,065.80	1,092.20
Carcharhinus plumbeus	Pelagic	69,800.00	2,350.00	3.37	12,900.00	18.48	65,786.99	13,679.75	20.79	943.00	1,061.00	1,091.98
Sphyrna tiburo	Pelagic	1,380.00	70.30	5.09	31.00	2.25	1,280.03	29.52	2.31	1,050.00	1,078.10	1,078.76

Sphyrna tiburo	Pelagic	2,000.00	113.00	5.65	51.70	2.59	1,844.00	50.69	2.75	1,020.00	1,084.60	1,086.43
Mustelus norrissi	bentho-pelagic	896.00	43.00	4.80	44.20	4.93	832.25	47.27	5.68	935.00	1,076.60	1,085.13
Mustelus norrissi	bentho-pelagic	876.00	41.90	4.78	46.70	5.33	813.98	48.24	5.93	968.00	1,076.20	1,083.02
Carcharhinus obscurus	Pelagic	238,300.00	4,450.00	1.87	49,400.00	20.73	228,541.29	52,553.19	23.00	940.00	1,042.70	1,073.37
Carcharhinus obscurus	Pelagic	188,900.00	5,030.00	2.66	27,200.00	14.40	179,341.12	28,661.75	15.98	949.00	1,053.30	1,073.14
Carcharhinus obscurus	Pelagic	5,500.00	116.00	2.11	1,040.00	18.91	5,254.61	1,121.90	21.35	927.00	1,079.19	1,079.19
Carcharhinus obscurus	Pelagic	5,580.00	116.00	2.08	1,080.00	19.35	5,332.57	1,161.29	21.78	930.00	1,078.81	1,078.81
Carcharhinus obscurus	Pelagic	6,580.00	345.00	5.24	260.00	3.95	6,108.43	260.00	4.26	1,000.00	1,077.20	1,080.63
Carcharhinus obscurus	Pelagic	4,410.00	227.00	5.15	219.00	4.97	4,085.60	220.77	5.40	992.00	1,079.40	1,084.39
Carcharhinus leucas	Pelagic	172,700.00	5,220.00	3.02	25,800.00	14.94	164,054.34	27,243.93	16.61	947.00	1,052.70	1,073.75
Carcharhinus leucas	Pelagic	127,900.00	4,890.00	3.82	13,000.00	10.16	120,501.22	13,698.63	11.37	949.00	1,061.40	1,075.82
Carcharhinus leucas	Pelagic	123,800.00	5,140.00	4.15	13,900.00	11.23	116,233.22	14,464.10	12.44	961.00	1,065.10	1,079.90
Carcharhinus leucas	Pelagic	117,900.00	4,150.00	3.52	16,500.00	13.99	111,236.91	17,497.35	15.73	943.00	1,059.90	1,081.72
Carcharhinus leucas	Pelagic	57,100.00	2,800.00	4.90	2,420.00	4.24	53,304.71	2,372.55	4.45	1,020.00	1,071.20	1,073.59
Carcharhinus leucas	Pelagic	118,400.00	5,020.00	4.24	7,570.00	6.39	111,288.65	7,820.25	7.03	968.00	1,063.90	1,071.15
Sphyrna mokarran	Pelagic	37,600.00	1,840.00	4.89	1,440.00	3.83	35,055.01	1,441.44	4.11	999.00	1,072.60	1,075.76
Sphyrna mokarran	Pelagic	141,000.00	6,660.00	4.72	13,400.00	9.50	131,321.60	13,914.85	10.60	963.00	1,073.70	1,086.82
Carcharhinus falciformis	Pelagic	3,760.00	181.00	4.81	161.00	4.28	3,500.28	157.84	4.51	1,020.00	1,074.20	1,076.76

Carcharhinus falciformis	Pelagic	6,490.00	327.00	5.04	246.00	3.79	6,023.76	246.00	4.08	1,000.00	1,077.40	1,080.70
Rhizoprionodon terranoeva	Pelagic	976.00	50.80	5.20	40.10	4.11	904.79	39.31	4.35	1,020.00	1,078.70	1,081.37
Carcharhinus limbatus	Pelagic	26,800.00	1,500.00	5.60	1,430.00	5.34	24,803.33	1,469.68	5.93	973.00	1,080.50	1,087.27
Mustelus Asterias	bentho-pelagic	2,050.00	78.50	3.83	154.70	7.20	1,920.60	156.75	8.16	986.95	1,067.37	1,074.52
Mustelus Asterias	bentho-pelagic	2,520.00	98.00	3.89	186.20	7.40	2,359.47	190.65	8.08	976.67	1,068.03	1,076.07
Mustelus Asterias	bentho-pelagic	762.50	30.00	3.94	35.30	4.60	713.59	35.36	4.96	998.22	1,068.54	1,072.21
Mustelus Asterias	bentho-pelagic	599.00	27.50	4.59	23.50	3.90	556.75	22.99	4.13	1,022.15	1,075.89	1,078.21
Cephasciolum ventriosum	demersal	1,521.00	63.00	4.14	105.00	6.90	1,420.36	101.32	7.13	1,036.37	1,070.85	1,073.50

Table S2. Fin morphometrics of a bull shark taken from the scientific drawings presented in Castro, 2011. The original data were for a 2 m total length animal (standard length = ~1.5m). All measurements were extracted using ImageJ. We scaled these measurements to an animal of 1m SL assuming isometry to conform with our density data.

	1.5 m Standard Length			1 m Standard Length		
	Area (m^2)	Length (m)	Chord (m)	Area (m^2)	Length (m)	Chord (m)
Pectorals	0.045	0.372	0.205	0.020	0.248	0.137
Dorsal 1	0.039	0.335	0.24	0.017	0.223	0.160
Pelvic	0.007	0.101	0.106	0.003	0.067	0.071
Dorsal 2	0.007	0.008	0.183	0.003	0.005	0.122
Anal	0.006	0.15	0.078	0.003	0.100	0.052

Table S3. Caudal Fin morphometrics of a Bull Shark taken from the scientific drawings presented in Castro, 2011. The original data were for a 2 m total length animal (standard length = ~1.5m). All measurements were extracted using ImageJ. We scaled these measurements to an animal of 1m SL assuming isometry.

Upper Caudal Lobe	**1.5 m Standard Length**	**1 m Standard Length TL**
FCA (m)	0.16	0.11
FCB (m)	0.12	0.21
h	0.25	0.17
Lower Caudal Lobe		
FCA (m)	0.16	0.11
FCB (m)	0.08	0.05
h (m)	0.18	0.12

Table S4. Fin morphometrics of a smooth dogfish taken from the scientific drawings presented in Castro, 2011. The original data were for a 1.13 m total length animal. All measurements were extracted using ImageJ. We scaled these measurements to a size of 0.44 m to correspond to the measurements of Andersen et al.. All scaling assumed isometry.

	1.13m Total Length			0.44m Total Length		
	Area (m^2)	Length (m)	Chord (m)	Area (m^2)	Length (m)	Chord (m)
Pectorals	0.045	0.372	0.205	0.020	0.248	0.137
Dorsal 1	0.039	0.335	0.24	0.017	0.223	0.160
Pelvic	0.007	0.101	0.106	0.003	0.067	0.071
Dorsal 2	0.007	0.008	0.183	0.003	0.005	0.122
Anal	0.006	0.15	0.078	0.003	0.100	0.052

Table S5. Caudal Fin morphometrics of a smooth dogfish taken from the scientific drawings presented in Castro, 2011. The original data were for a 1.13 m total length animal. All measurements were extracted using ImageJ. We scaled these measurements to a size of 0.44 m to correspond to the measurements of Andersen et al. All scaling assumed isometry.

Upper Caudal Lobe	**1.13m TL**	**0.44m TL**
FCA (m)	0.077	0.030
FCB (m)	0.118	0.046
h	0.125	0.049
Lower Caudal Lobe		
FCA (m)	0.077	0.030
FCB (m)	0.08	0.031
h (m)	0.23	0.090